Available online at www.sciencedirect.com
SCIENCE DIRECT®
Planetary and Space Science 54 (2006) 967–987
Planetary and Space Science

In situ dust measurements in the inner Saturnian system

R. Srama[a,*], S. Kempf[a], G. Moragas-Klostermeyer[a], S. Helfert[a], T.J. Ahrens[b], N. Altobelli[c], S. Auer[d], U. Beckmann[a], J.G. Bradley[c], M. Burton[c], V.V. Dikarev[a], T. Economou[e], H. Fechtig[a], S.F. Green[f], M. Grande[g], O. Havnes[h], J.K. Hillier[f], M. Horanyi[i], E. Igenbergs[j], E.K. Jessberger[k], T.V. Johnson[c], H. Krüger[l], G. Matt[a], N. McBride[f], A. Mocker[a], P. Lamy[m], D. Linkert[a], G. Linkert[a], F. Lura[n], J.A.M. McDonnell[f], D. Möhlmann[n], G.E. Morfill[o], F. Postberg[a], M. Roy[c], G.H. Schwehm[p], F. Spahn[q], J. Svestka[r], V. Tschernjawski[n], A.J. Tuzzolino[e], R. Wäsch[n], E. Grün[a,s]

[a]*Max Planck Institute Nuclear Physics, Heidelberg, Germany*
[b]*Seismological Laboratory, CALTECH, Pasadena, USA*
[c]*Jet Propulsion Laboratory, Pasadena, USA*
[d]*A & M Associates, Basye, USA*
[e]*Enrico Fermi Institute, University of Chicago, Chicago, USA*
[f]*Open University, Milton Keynes, UK*
[g]*Rutherford Appleton Laboratory, Chilton, Didcot, Oxon, UK*
[h]*Auroral Observatory, University of Tromso, Tromso, Norway*
[i]*University of Colorado, Boulder, USA*
[j]*Technical University of Munich, Garching, Germany*
[k]*University of Mnster, Mnster, Germany*
[l]*Max Planck Institute Solar System Research, Kathlenburg-Lindau, Germany*
[m]*Laboratoire dAstronomie Spatiale, Marseille, France*
[n]*DLR, Berlin, Germany*
[o]*Max Planck Institute Physics and Astronomy, Garching, Germany*
[p]*ESA-ESTEC, Noordwijk, The Netherlands*
[q]*University of Potsdam, Potsdam, Germany*
[r]*Prague Observatory, Prague, Czech Republic*
[s]*HIGP, University of Hawaii, Honolulu, Hawaii, USA*

Accepted 4 May 2006
Available online 26 July 2006

Abstract

In July 2004 the Cassini–Huygens mission reached the Saturnian system and started its orbital tour. A total of 75 orbits will be carried out during the primary mission until August 2008. In these four years Cassini crosses the ring plane 150 times and spends approx. 400 h within Titan's orbit. The Cosmic Dust Analyser (CDA) onboard Cassini characterises the dust environment with its extended E ring and embedded moons. Here, we focus on the CDA results of the first year and we present the Dust Analyser (DA) data within Titan's orbit. This paper does investigate High Rate Detector data and dust composition measurements. The authors focus on the analysis of impact rates, which were strongly variable primarily due to changes of the spacecraft pointing. An overview is given about the ring plane crossings and the DA counter measurements. The DA dust impact rates are compared with the DA boresight configuration around all

*Corresponding author. Tel.: +49 6221 516423; fax: +49 6221 516601.
E-mail address: ralf.srama@mpi-hd.mpg.de (R. Srama).

0032-0633/$ - see front matter
doi:10.1016/j.pss.2006.05.021

ring plane crossings between June 2004 and July 2005. Dust impacts were registered at altitudes as high as 100 000 km above the ring plane at distances from Saturn between 4 and 10 Saturn radii. In those regions the dust density of particles bigger than 0.5 μm can reach values of $0.001\,m^{-3}$.

Keywords: Cassini; Dust; CDA; E-ring; Water ice

1. Introduction

The Cosmic Dust Analyser (CDA) onboard Cassini was put into operation in 1999 and has since achieved many outstanding scientific discoveries. Its success started during the interplanetary cruise where the instrument discovered interstellar dust at Earth distance (Altobelli et al., 2003). This discovery was followed by a chemical analysis of the jovian dust stream particles (Postberg et al., 2006) and the first measurement of electrical charges on interplanetary dust particles (Kempf et al., 2004). Afterwards, during the approach to Saturn, the CDA instrument discovered Saturn's dust streams. These particles are jettisoned into interplanetary space with speeds of approximately $100\,km\,s^{-1}$ and originate from Saturn's ring system (Kempf et al., 2005 a,b). It was shown that beyond Saturn's E ring, even the outer main ring acts as a dust source for stream particles. Furthermore, the integrated time-of-flight mass spectrometer allowed an elemental analysis of those tiny, nanometre sized grains.

At the time of writing, Cassini has been investigating the Saturnian system for one year and the dust instrument has continued operating successfully, starting its exploration of Saturns dusty environment. The main task of CDA is the investigation of Saturn's E ring and the interaction of ring particles with the embedded moons Mimas, Enceladus, Tethys, Dione and Rhea. It is well known that the moons are bombarded by interplanetary and ring particles leading to the release of secondary ejecta which will become ring particles themselves under certain conditions (Spahn et al., 1999; Krüger et al., 2000). However, there is one specific moon dominating the formation of Saturn's E ring. This moon is Enceladus, located at a distance of 3.95 Saturn radii (R_S, $1R_S = 60280\,km$), having a diameter of 500 km and a surface composed of pure water ice. The recent close flyby of Cassini at this moon on July 14, 2005, allowed us a detailed study of the dust density distribution in the vicinity of Enceladus. Enceladus is not only acting as a passive source for ring particles (the bombardment of particles releases secondary projectiles), but also an active source: geologic activities on the southern hemisphere of Enceladus (geysers, ice volcanoes) produce icy grains which leave the gravitational influence of Enceladus and become ring particles (Spahn et al., 2006). This discovery was a major step for the understanding of the ring formation. In this paper, we summarise the dust measurements in the E ring region of Saturn.

2. Mission events

After a close flyby of Phoebe on June 11, 2004, Cassini entered the Saturnian system on July 1st, 2004 (Day-of-year, DOY 183). During its first orbit, Cassini came as close as 1.3 Saturn radii to the planet. In the following year until July 2005, Cassini performed 14 orbits around Saturn. Cassini uses the moon Titan to change the orbit geometry (inclination, phase angle) and Cassini's apocentre distance changed from $150R_S$ down to $40R_S$ in orbit 11. During each orbit, three prime orbit trim manoeuvres (OTM) are planned with the same number of backup windows. Tables 1 and 2 give a list with the main mission events like pericentres, ring plane crossing, OTMs, dust hazard regions (high-gain antenna to the relative dust impact direction: HGA to RAM) satellite flybys and apocentres. The tables are relevant for a later discussion of possible instrument contaminations during OTMs by main engine plumes. During this time period five Titan flybys (TI), three targeted Enceladus flybys (EN) and one Phoebe flyby (PH) occurred. The best flyby geometry for dust measurements was achieved during the last Enceladus flyby on July 14 in 2005 (DOY 195).

We define the E ring region as a torus of wedge-shaped cross-section of radius between 3 and $18R_S$ and ±20 latitude. In the time frame discussed, Cassini entered Saturn's E ring region 13 times at different distances and latitudes. Table 3 gives an overview of the measurement phases in the inner Saturnian system with an outer distance boundary of $18R_S$ and a latitude boundary of 20. The table shows the entry and exit times in Spacecraft Event Time (SCET), the distances and latitudes during entry and exit, and the minimum distance to Saturn during this phase (pericentre).

3. CDA instrument and operations

The CDA determines the speed, mass and composition of individual dust grains. The instrument has two subsystems, the High Rate Detector (HRD) provided by the University of Chicago, and the Dust Analyser (DA) developed by the Max Planck Institute Nuclear Physics in Heidelberg and the University of Kent in Canterbury (group now at The Open University). The HRD uses thin foils for the dust detection and can measure high impact rates of particles bigger than approximately 2 μm. In this paper, only results of the DA subsystem are reported. The DA instrument is based on impact ionisation of

Table 1
Cassini mission events during the year 2004 (OTM = Orbit Trim Maneuver, Per = Periapsis, inc = inclination, r = radius, v = velocity, ME = Main Engine, HGA = High Gain Antenna, RCS = Reaction Control System)

Seq.	Rev.	Name	Epoch (SCET)	Date	050720, version 9/20/05 Comment
S1	0	00PH (t)	2004-163T19:34	11.06.2004	2071 km flyby, $v = 6.4\,\mathrm{km\,s^{-1}}$
S2	0	2.68_Rs	2004-183T00:44	01.07.2004	End 183T00:49(00:05) HGA to RAM
S2	0	Ring CRX	2004-183T00:46	01.07.2004	$r = 2.63R_s$
S2	0	SOI Start	2004-183T01:12	01.07.2004	SOI burn, delta$V = 626\,\mathrm{m\,s^{-1}}$, duration = 01 : 36 : 20
S2	0	Periapse	2004-183T02:38	01.07.2004	Per = 6192.5 d, inc = 17.2°, $r = 1.3R_s$
S2	0	SOI End	2004-183T02:48	01.07.2004	SOI burn end
S2	0	2.68_Rs	2004-183T04:31	01.07.2004	End 183T04:36(00:05) HGA to RAM
S2	0	Ring CRX	2004-183T04:34	01.07.2004	$r = 2.63R_s$
S3	0	OTM-002	2004-236T09:53	23.08.2004	delta$V = 393\,\mathrm{m\,s^{-1}}$, ME, duration = 3050 s
S3	a	Apoapse	2004-240T08:57	27.08.2004	Per = 124.1 d, inc = 17.6°, $r = 150.8R_s$
S3	a	OTM-003	2004-251T10:30	07.09.2004	ME, duration = 4 s
S5	a	OTM-004	2004-297T00:16	23.10.2004	RCS, duration = 470 s
S5	a	0ATI (t)	2004-300T15:30	26.10.2004	[TA] 1174 km flyby, $v = 6.1\,\mathrm{km\,s^{-1}}$
S5	a	Ring CRX	2004-300T16:53	26.10.2004	$r = 19.51R_s$
S5	a	Periapse	2004-302T10:20	28.10.2004	Per = 47.9 d, inc = 13.8°, $r = 6.2R_s$
S5	a	Ring CRX	2004-302T20:01	28.10.2004	$r = 8.08R_s$
S5	a	OTM-005	2004-303T00:15	29.10.2004	ME, duration = 5 s
S6	a	OTM-006	2004-325T23:00	20.11.2004	ME, duration = 3 s
S6	b	Apoapse	2004-326T08:41	21.11.2004	Per = 47.9 d, inc = 13.8°, $r = 78.1R_s$
S6	b	0BTI (t)	2004-348T11:38	13.12.2004	[TB] Inbound 1192 km flyby, $v = 6.1\,\mathrm{km\,s^{-1}}$
S6	b	Ring CRX	2004-348T14:57	13.12.2004	$r = 18.86R_s$
S6	b	Periapse	2004-350T05:51	15.12.2004	Per = 32.1 d, inc = 5.2°, $r = 4.8R_s$
S6	b	Ring CRX	2004-350T11:03	15.12.2004	$r = 5.75R_s$
S7	b	OTM-008	2004-351T19:22	16.12.2004	Probe targeting, delta$V = 16\,\mathrm{m\,s^{-1}}$, ME, 85 s
S7	b	OTM-009	2004-357T18:52	22.12.2004	Probe targeting cleanup, RCS, 16 s
S7	b	Probe Release	2004-360T02:00	25.12.2004	At entry interface—20.3 d
S7	b	OTM-010	2004-362T18:37	27.12.2004	Orbit deflection, delta$V = 24\,\mathrm{m\,s^{-1}}$, ME, 153 s
S7	c	Apoapse	2004-366T07:02	31.12.2004	Per = 31.9 d, inc = 5.3°, $r = 59.7R_s$

Table 2
Cassini mission events during the year 2005 until DOY 200

Seq.	Rev.	Name	Epoch (SCET)	Date	050720, version 9/20/05 Comment
S7	c	OTM-010A	2005-003T17:38	03.01.2005	RCS, 148 s
S7	c	Ring CRX	2005-014T17:04	14.01.2005	$r = 18.36R_s$
S7	c	OTM-011	2005-016T03:20	16.01.2005	ME, 140 s
S7	c	Periapse	2005-016T06:25	16.01.2005	Per = 33.5 d, inc = 5.2°, $r = 4.8R_s$
S7	c	Ring CRX	2005-016T11:58	16.01.2005	$r = 5.90R_s$
S8	c	OTM-012	2005-028T01:08	28.01.2005	ME, 120 s
S8	3	Apoapse	2005-032T03:26	01.02.2005	Per = 31.8 d, inc = 5.2°, $r = 59.3R_s$
S8	3	OTM-013	2005-043T00:07	12.02.2005	RCS, 220 s
S8	3	03TI (t)	2005-046T06:58	15.02.2005	[T3] Inbound 1579 km flyby, $v = 6.0\,\mathrm{km\,s^{-1}}$
S8	3	Ring CRX	2005-048T00:50	17.02.2005	$r = 3.50R_s$
S8	3	Periapse	2005-048T00:57	17.02.2005	Per = 20.7 d, inc = 0.4°, $r = 3.5R_s$
S8	3	03EN (t)	2005-048T03:30	17.02.2005	[E1] Outbound 1264 km flyby, $v = 6.7\,\mathrm{km\,s^{-1}}$
S8	3	OTM-014	2005-049T00:00	18.02.2005	ME, 5 s
S8	3	Ring CRX	2005-057T04:44	26.02.2005	$r = 43.98R_s$
S9	4	Apoapse	2005-058T06:20	27.02.2005	Per = 20.5 d, inc = 0.4°, $r = 44.3R_s$
S9	4	OTM-015	2005-060T22:50	27.02.2005	ME, 40 s
S9	4	04EN (t)	2005-068T09:08	09.03.2005	[E2] Inbound 501 km flyby, $v = 6.6\,\mathrm{km\,s^{-1}}$
S9	4	E_ring_lg	2005-068T09:18	09.03.2005	End 068T11:02 HGA to RAM
S9	4	Ring CRX	2005-068T10:48	09.03.2005	$r = 3.56R_s$
S9	4	Periapse	2005-068T11:40	09.03.2005	Per = 20.8 d, inc = 0.2°, $r = 3.5R_s$
S9	4	OTM-017	2005-070T21:20	11.03.2005	ME, 3 s
S9	4	Ring CRX	2005-073T17:01	14.03.2005	$r = 36.95R_s$
S9	4	OTM-018	2005-078T12:19	19.03.2005	ME, 10 s
S9	5	Apoapse	2005-078T17:35	19.03.2005	Per = 20.5 d, inc = 0.2°, $r = 44.4R_s$
S9	5	Ring CRX	2005-088T22:59	29.03.2005	$r = 3.53R_s$

Table 2 (*continued*)

Seq.	Rev.	Name	Epoch (SCET)	Date	050720, version 9/20/05 Comment
S9	5	Periapse	2005-088T23:38	29.03.2005	Per = 20.8 d, inc = 0.3°, $r = 3.5R_s$
S9	5	05TI (t)	2005-090T20:05	31.03.2005	[T4] Outbound 2404 km flyby, $v = 5.9\,km\,s^{-1}$
S9	5	Ring CRX	2005-090T22:06	31.03.2005	$r = 21.28R_s$
S9	5	OTM-020	2005-093T20:22	03.04.2005	ME, 6 s
S9	6	Apoapse	2005-096T23:32	06.04.2005	Per = 16.0 d, inc = 7.4°, $r = 38.0R_s$
S10	6	OTM-021	2005-099T20:00	09.04.2005	ME, 37 s
S10	6	OTM-022	2005-103T20:40	13.04.2005	RCS, 70 s
S10	6	G_ring	2005-104T22:12	14.04.2005	End 104T22:16(00:04) HGA to RAM
S10	6	Ring CRX	2005-104T22:16	14.04.2005	$r = 2.73R_s$
S10	6	Periapse	2005-104T23:16	14.04.2005	Per = 16.4 d, inc = 7.6°, $r = 2.6R_s$
S10	6	06TI (t)	2005-106T19:12	16.04.2005	[T5] Outbound 1026 km flyby, $v = 6.1\,km\,s^{-1}$
S10	6	Ring CRX	2005-106T19:58	16.04.2005	$r = 20.89R_s$
S10	7	Apoapse	2005-113T23:30	23.04.2005	Per = 18.2 d, inc = 21.7°, $r = 40.6R_s$
S10	7	OTM-024	2005-118T18:58	28.04.2005	ME, 13 s
S10	7	Ring CRX	2005-122T23:36	02.05.2005	$r = 3.90R_s$
S10	7	Periapse	2005-123T01:43	03.05.2005	Per = 18.4 d, inc = 21.9°, $r = 3.6R_s$
S10	7	Ring CRX	2005-125T02:08	05.05.2005	$r = 21.42R_s$
S10	8	Apoapse	2005-132T03:52	12.05.2005	Per = 18.2 d, inc = 21.9°, $r = 40.6R_s$
S11	8	Ring CRX	2005-141T03:54	21.05.2005	$r = 3.90R_s$
S11	8	Periapse	2005-141T06:02	21.05.2005	Per = 18.4 d, inc = 21.9°, $r = 3.6R_s$
S11	8	Ring CRX	2005-143T05:45	23.05.2005	$r = 21.23R_s$
S11	9	Apoapse	2005-150T08:21	30.05.2005	Per = 18.2 d, inc = 21.9°, $r = 40.6R_s$
S11	9	Ring CRX	2005-159T08:26	08.06.2005	$r = 3.91R_s$
S11	9	Periapse	2005-159T10:36	08.06.2005	Per = 18.4 d, inc = 21.9°, $r = 3.6R_s$
S11	9	Ring CRX	2005-161T09:08	10.06.2005	$r = 20.90R_s$
S11	10	Apoapse	2005-168T13:12	17.06.2005	Per = 18.2 d, inc = 21.8°, $r = 40.7R_s$
S12	10	Ring CRX	2005-177T13:29	26.06.2005	$r = 3.93R_s$
S12	10	Periapse	2005-177T15:42	26.06.2005	Per = 18.4 d, inc = 21.8°, $r = 3.6R_s$
S12	10	Ring CRX	2005-179T13:45	28.06.2005	$r = 20.76R_s$
S12	11	Apoapse	2005-186T18:58	05.07.2005	Per = 18.3 d, inc = 21.8°, $r = 40.7R_s$
S12	11	OTM-025	2005-189T14:37	08.07.2005	ME, 2 s
S12	11	11PM (nt)	2005-195T19:31	14.07.2005	Inbound 122 213 km flyby, $v = 6.1\,km\,s^{-1}$
S12	11	E_ring_lg	2005-195T19:55	14.07.2005	End 195T19:57
S12	11	11EN (t)	2005-195T19:55	14.07.2005	[E3] Inbound 172 km flyby, $v = 8.2\,km\,s^{-1}$
S12	11	Ring CRX	2005-195T19:56	14.07.2005	$r = 3.95R_s$
S12	11	11ME (nt)	2005-195T20:47	14.07.2005	Inbound 36 690 km flyby, $v = 7.6\,km\,s^{-1}$
S12	11	11EP (nt)	2005-195T20:55	14.07.2005	Inbound 76 782 km flyby, $v = 6.3\,km\,s^{-1}$
S12	11	Periapse	2005-195T22:10	14.07.2005	Per = 18.5 d, inc = 21.8°, $r = 3.6R_s$
S12	11	Ring CRX	2005-197T19:44	16.07.2005	$r = 20.63R_s$

hypervelocity particles: an impact of a particle at a few $km\,s^{-1}$ onto the hemispherical gold target (Impact Ionisation Detector, IID) with a sensitive area of $0.1\,m^2$ produces ejecta, neutral atoms and an impact plasma of ions and electrons. The plasma is separated in an electric field and the positive ions are accelerated towards the ion grid (signal QI) and the multiplier (signal QM). The electrons are collected at the target and generate the signals QT and QC (see below). A further channel measures the induced charge of grains flying through the CDA entrance grid system (QP, Kempf et al., 2004). The integrated time-of-flight mass spectrometer consists of the Chemical Analyser Target (CAT, signal QC), an acceleration grid and the multiplier at a distance of 23 cm. Further instrument details are given in Bradley et al. (1996), Srama et al. (2004) and Ratcliff et al. (1992). The sensitive area of the DA target is dependent on the incident angle. A normal incidence gives a high sensitive area of almost $0.09\,m^2$ (compare Table 4).

Raw data from a water ice particle impact onto the chemical analyser are shown in Fig. 1. This event was registered at $12.7R_s$ distance and 2.3 latitude. The relative impact speed for circular prograde particles at this location is $7.6\,km\,s^{-1}$.

Charge signals of an impact onto the IID which occurred at 2005-141T21:05 are plotted in Fig. 2. At this time Cassini was at a Saturn distance of $9.7R_s$ and a latitude of 11.7. Such an event corresponds in all aspects to impact signals obtained during laboratory measurements. Mass spectra of water ice particles were recorded at high latitudes.

The mass threshold M_T of the instrument is dependent on the impact speed v and is approximately given by

$$M_T\,(kg) = 3.037 \times 10^{-13} \cdot v^{-3.752}\,(km\,s^{-1}). \quad (1)$$

This function was established during laboratory measurements with iron particles and depends on the projectile

Table 3
Entry and exit times of Cassini in the inner Saturnian region inside $18R_s$ and ±20 latitude

SCET-entry	SCET-exit	R_s-entry	Lat-entry	R_s-exit	Lat-exit	Per (R_s)
2004-182/02:25:00	2004-184/06:15:00	18.24	−14.20	17.98	−14.99	1.33
2004-300/21:19:59	2004-303/22:54:59	18.03	0.88	17.88	−11.10	6.18
2004-348/17:29:59	2004-351/18:09:59	18.02	0.17	18.00	−5.02	4.77
2005-014/17:59:59	2005-017/18:44:59	18.06	0.07	17.96	−4.97	4.83
2005-046/12:44:59	2005-049/12:39:59	18.11	−0.28	17.94	0.26	3.50
2005-066/23:24:59	2005-069/23:24:59	18.12	−0.19	17.96	0.09	3.51
2005-087/11:24:59	2005-090/11:19:59	18.11	−0.24	17.94	0.14	3.50
2005-103/11:49:59	2005-106/10:09:59	18.09	−6.56	17.92	0.76	2.60
2005-122/14:49:59	2005-123/03:39:59	7.83	−20.05	3.86	19.92	3.59
2005-123/08:09:59	2005-124/14:29:59	5.68	20.09	18.00	2.47	5.68
2005-140/19:04:59	2005-141/07:59:59	7.86	−20.02	3.86	19.99	3.60
2005-141/12:29:59	2005-142/18:44:59	5.68	20.02	17.97	2.36	5.68
2005-158/23:24:58	2005-159/12:29:58	7.98	−20.03	3.84	19.87	3.59
2005-159/16:54:58	2005-160/23:19:58	5.61	20.06	17.98	2.14	5.61
2005-177/04:19:58	2005-177/17:34:58	8.06	−20	3.85	19.84	3.61
2005-177/21:59:58	2005-179/04:29	5.60	20.0	18.0	2.03	5.60
2005-195/10:34:58	2005-196/00:04:58	8.16	−20.0	3.86	20.0	3.61
2005-196/04:24:58	2005-197/10:54:58	5.59	20.0	18.0	1.94	5.59

If Cassini exits the ±20 region, the orbit segment is split up into two segments (e.g. around 2005-177).

Table 4
Total effective sensitive area of the DA instrument in dependence of the incident angle (0° = normal incidence)

Angle (°)	Area (m^2)
0	0.0900
5	0.0800
10	0.0700
15	0.0578
20	0.0467
25	0.0360
30	0.0250
35	0.0152
40	0.0073
45	0.0016
50	0.000

The areas calculated take into account the special sensor geometry (obscuration by the multiplier housing). The CDA mounting geometry onboard Cassini is described in Srama et al. (2004).

material and the current threshold settings of the CDA instrument. Since the threshold settings onboard Cassini are lower than or equal to the settings of the former laboratory measurements, one can assume that this formula is quite conservative for the estimation of the lower mass limit.[1] Assuming a typical relative impact speed of $8\,km\,s^{-1}$, the lower mass threshold would be 1.2×10^{-16} kg. This mass corresponds to compact water ice particles with a diameter of 0.6 μm. Faster impact speeds decrease this mass threshold significantly: impact speeds of $20\,km\,s^{-1}$ already produce enough impact charge for water ice grains with diameters above 200 nm to be detected. Such velocities are easily reached and exceeded by Saturn stream particles (Kempf et al., 2005b). Furthermore, stream particle impacts onto the chemical analyser produce mass spectra and the high hydrogen peak of the spectra can release the event trigger at the multiplier channel. By this means high-velocity ($>100\,km\,s^{-1}$) particles down to sizes of a few nanometre can be detected by the DA instrument!

The CDA instrument is generally switched on and in a measurement configuration all the time. The measurement times are interrupted by short periods (max. 40 min, approximately once per day) during articulations of the CDA platform, by checkout phases (a few hours of duration), by CDA decontaminations (duration approximately 12 h), by orbit manoeuvres (approximately 4 h for each OTM) and segments of CDA anomalies (reset and reboot of the instrument after interrupt problems or commanding errors). The CDA switch-off times are limited to the time intervals 2004-173T22:30–2004-183T17:00 (CDA switch off during Saturn Orbit Insertion) and 2005-006T1 1:40–2005-015T11:35 (Huygens probe mission).

3.1. Target decontaminations and flight software updates

Decontamination is performed by heating the small CAT up to 100 °C for approximately 8 h by a dedicated heater which consumes approximately 5 W. The four CDA decontaminations within the time window discussed in this paper started at the times (SCET) 2004-284T08:46, 2005-039T21:23, 2005-130T21:34 and 2005-146T04:19. The target heating is necessary in order to clean the target surface of any contaminations which might occur due to

[1]The threshold deviations between laboratory and flight do not exceed a factor of two.

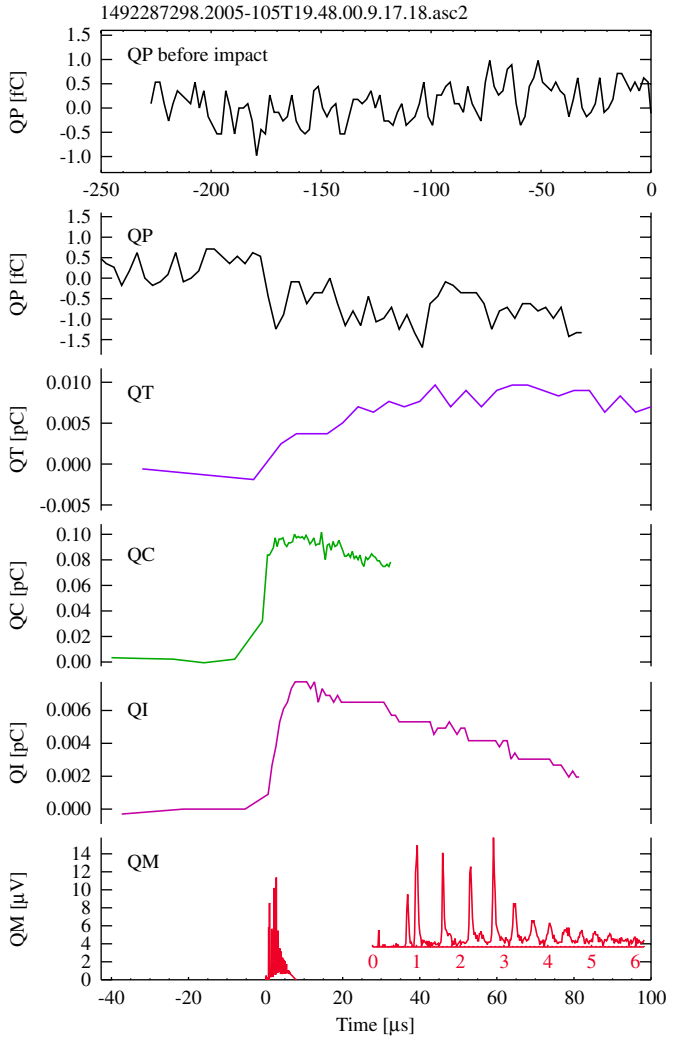

Fig. 1. Raw impact signals of a water ice particle at 12.7R_s and 2.3 latitude. The signals from the entrance grid (QP), the electron signal of the big gold target of the IID (QT), the electron signal of the small chemical analyser target (QC), the ion signal of the ion grid (QI) and the multiplier signal (QM) are shown. The impact trigger occurred at the time 0. This impact occurred on the chemical analyser target and produced a characteristic mass spectrum at the multiplier (zoomed signal at the lower right with the same units). The spectrum shows the characteristic clustering of water molecules as described in Hillier et al. (2006).

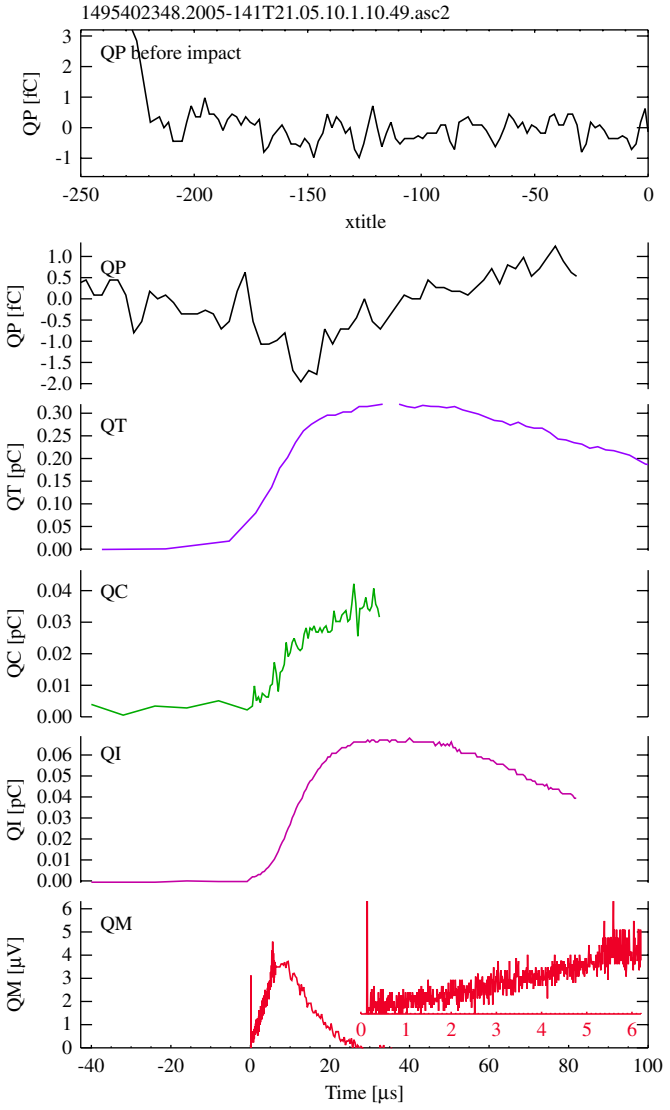

Fig. 2. Raw impact signal data from a dust impact at 9.7R_s and 11.7 latitude. The impact occurred on the big gold target and shows a strong electron signal on the channel QT.

outgassing materials or due to main engine firings. Most OTMs use the thrusters for small trajectory corrections and contamination is negligible. However, some OTMs use Cassini's main engine and plume residuals might reach the target section and cause contamination. The entry of plume molecules is minimal if the instrument aperture is articulated away from the main engine direction. Unfortunately, the firing of the main engine is decided very late in the sequencing process so CDA was articulated to a safe position during each OTM prime and backup window (six times in each orbit). During the preparation phase of the instrument uplink commands, the pointing of CDA is optimised by using the articulation mechanism and the data rates are adjusted according to the onboard telemetry modes. For CDA prime observations, the instrument team prepares the pointing commands for the spacecraft using a special project-provided tool (Pointing Design Tool, PDT).

During the long operations phase of CDA, several adjustments of the onboard flight software (FSW) were necessary. This ongoing development has four causes. First, the Cassini onboard software capabilities and modes changed with time. Second, the cruise and early tour data provided input for a better impact signal analysis and event handling. Third, the risk for operations has to be as low as possible and some command sequences were streamlined by using sophisticated commanding procedures (Instrument Extended Blocks). Finally, the instrument found much more dust in Saturn's environment than originally expected. Therefore, the utilisation of the available data

volume is critical and must be as efficient as possible. CDAs data rate varies between 100 and 4192 bps. Outside Titan's orbit the data rate is typically lower than 300 bps. Without a complete transfer of raw data, the discovery and analysis of Saturn stream particles would not have been possible. Stream particles can be as small as 5 nm and they produce very small impact charges. On the other hand, they are seen in very extended regions around Saturn (from within Titan's orbit up to apocentre distances). The small signals also require the CDA measurement thresholds to be set as low as possible which increases the overall amount of raw data (real impacts plus noise). Therefore, it is necessary to transfer both signals with high amplitudes (big impacts) and as much noise data including many hidden stream particle impacts as possible. Some major FSW updates onboard Cassini's solid state recorder were made at 2004-124 (FSW version 9.2), 2004-215 (FSW version 9.2.4) and 2005-142 (FSW version 10.0). The corresponding instrument checkouts occurred a few days later.

3.2. Counter formats and rate definitions

The instrument has five signal channels (QP, QC, QT, QI, QM) and all of them are monitored for amplitudes exceeding the individual channel threshold. Once an event is registered (trigger) the five signals are analysed and compressed by the onboard software. Signal baselines, amplitudes, integrals and risetimes are evaluated and are used for a complex classification scheme. Depending on the individual signal parameters, one of 20 counters is increased by 1. Table 5 shows the detailed classification scheme with a short description of the individual counters. The latest FSW 10.0 has been used since 2005-150 and has a new signal classification scheme and modified counter conditions. Based on the experience gained during the cruise phase, the classification was modified and the number of counters was increased from 20 to 27 (Table 6). Furthermore, the counters are correlated with counter classes. Counter class 0 reflects very tiny or noise events, class 1 is used for test pulses, class 2 stands for clear impact signals with medium amplitudes and class 3 includes counters of clear and big dust impacts. The counter classes are used to allow a balanced transmission of impact data to the ground. Raw data from events of all classes are downlinked to Earth, with a slight emphasis on events from class 2 and 3. This ensures that some noise data are returned and helps determine the noise behaviour of the instrument (class 0) even during days with a high impact rate. Class 3 events cannot overwrite data from another class and each class has the same memory depth. The bit length of the counters is restricted to 12 bits in the latest counter scheme. Counter snapshots are taken every 64 s and the dead time is 1 s. Some 8 bit counter can overflow after 256 s at the earliest, but the oversampling of counter values with a nominal period of 64 s allows the detection and correction of counter overflows.

Table 5
Counter classification scheme up to flight software version 9.2.4 (until 2005-150)

Counter #	Counter queue	Class	Description
0	1	1	Test pulse (ok)
1	1	1	Test pulse (bad)
2	3	3	Clear CAT impact (spectrum)
3	3	3	Clear CAT impact (spectrum)
4	—	—	Internal interrupt loss counter
5	0	0	No clear signals, high baseline
6	3	3	Big, fast IID impact
7	3	3	Big, slow IID impact
8	3	3	Big, fast CAT impact
9	2	3	Big, slow CAT impact
10	2	2	Small, fast IID impact
11	2	2	Small, slow IID impact
12	2	2	Small, fast CAT impact
13	2	2	Small, slow CAT impact
14	2	3	Big QI and QT signal
15	2	3	Big QI and QC signal
16	0	0	Strong QI signal (QI flare)
17	2	2	Small QI & QC signals are present
18	2	2	Small QI & QT signals are present
19	0	0	ELSE

Each event (dust impact or noise) increments one of 20 counters. The counters are grouped into counter queues in order to provide an efficient downlink scheme. The counters 0–9 are 8 bit counters, whereas the counters 10–19 are of 16 bit length. The class is introduced in this paper and depends on the amplitude and reliability of an event (big events belong to the highest class 3).

4. CDA data

The CDA instrument was in its measurement configuration for long time periods, which were only interrupted by the OTMs and decontaminations identified above. However, pointing changes of the Cassini spacecraft require articulations of the CDA instrument which lead to short interrupts in the data acquisition time. The aperture of the DA has a 45 half-cone angle and the Cassini spacecraft is three axis stabilised. Therefore, the instrument sensitivity for the dust impact direction (dust RAM) is strongly dependent on the spacecraft attitude and may be low for long periods. During the sequence generation phase the CDA articulation was optimised for the dust RAM direction of circular prograde dust orbits. Furthermore, during some downlink phases the Cassini high-gain antenna was pointing towards Earth and the bus performed a slow roll (approximately 30 min per revolution) about its long main axis (z-axis). Here, the CDA boresight was set almost perpendicular to the rotation axis in order to maximise the scanned area in three-dimensional space. Fig. 3 shows the Cassini trajectory and the measured in situ dust impact rate for the first orbits until day 150 in the year 2005. This rate was dead time corrected using the common formula $R = r/(1 - r \cdot \tau)$ with the measured impact rate r (in units of s^{-1}), the DA dead time τ of 1 s and the corrected impact rate R. The maximum rate in the plots below was set to $45\,s^{-1}$ since the rate correction

Table 6
Counter classification scheme in flight software version 10.0 (after 2005-150)

Counter #	Name	Counter queue	Class	Bits	Description
0	A0	3	3	8	Medium impact onto CAT, many peaks $QC > 2.0 \times 10^{-13}$ C
1	A1	3	2	8	Medium impact onto CAT, many peaks $QC > 8.7 \times 10^{-14}$ C
2	A2	3	3	8	Big impact onto CAT, some peaks $QC > 8.1 \times 10^{-13}$ C
3	A3	3	2	8	Medium impact onto CAT, some peaks $QC > 3.2 \times 10^{-13}$ C
4	A4	3	1	8	Small impact onto CAT, some peaks $QC > 8.7 \times 10^{-14}$ C
5	A5	2	1	8	Small impact onto CAT, some peaks $QC > 6.1 \times 10^{-14}$ C
6	A6	2	1	8	Small impact onto CAT, no peaks $QC > 6.1 \times 10^{-14}$ C
7	A7	2	2	8	Medium CAT impact $QC > 2.0 \times 10^{-13}$ C
16	A8	2	0	12	Very small CAT impact $QC > 2.2 \times 10^{-14}$ C
8	I0	3	3	8	Very big IID impact, $QT > 4.2 \times 10^{-12}$ C
9	I1	3	3	8	Big, fast IID impact, $QT > 1.1 \times 10^{-12}$ C
10	I2	3	2	8	Medium, fast IID impact, $QT > 3.4 \times 10^{-13}$ C
17	I3	2	1	12	Small, fast IID impact, $QT > 3.1 \times 10^{-14}$ C
11	I4	3	3	8	Big, slow IID impact, $QT > 1.1 \times 10^{-12}$ C
12	I5	3	2	8	Medium, slow IID impact, $QT > 3.4 \times 10^{-13}$ C
18	I6	2	1	12	Small, slow IID impact, $QT > 3.1 \times 10^{-14}$ C
19	I7	2	0	12	Very small IID impact, $QT > 2.0 \times 10^{-14}$ C
20	W0	0	0	12	Big wall impact, $QI > 1.7 \times 10^{-14}$ C
21	W1	0	0	12	Small wall impact, $QI > 2 \times 10^{-15}$ C
13	B0	0	0	8	QC, QT and QI signals (both targets)
22	N0	0	0	12	No signals, high baseline
14	N1	1	0	8	Strong QI signal (QI flare) $QI > QC$, $QI > QT$, $QI > 5.3 \times 10^{-15}$ C
23	N2	0	0	12	Noise (ELSE)
24	T0	1	—	4	Test pulse ok
25	T1	1	—	4	Test pulse bad
15	S0	—	—	8	Spare (unused)
26	E0	0	—	8	Interrupt counter

Each event (dust impact or noise) increments one of 27 counters. The counters are grouped into counter queues to provide an efficient downlink scheme. The events are classified into four classes (class 0, 1, 2 and 3) dependent on the amplitude and reliability of an event. The highest classes 2 and 3 are very reliable and reflect big impact charges. The counter bit lengths are different in order to fit within the CDA housekeeping scheme. More abundant counters have a higher bit length. Wall impacts are identified by a special processing routine of the QP channel. Fast IID impacts have a target risetime below 40 μs (8.8 km s^{-1}). The trigger thresholds of the relevant target are given in Coulomb (QC, QT).

becomes inaccurate for higher rates. For the rate calculation only counters with a very low noise level have been taken into account. Therefore, counters 0, 1, 4, 5, 16 and 19 were not considered in this plot (see the counter definition in Table 5). All rates shown in this paper are based on counters which are corrected for overflow.

4.1. Data of ring plane crossings

The main topic of this paper is to present the data from the Cassini ring plane crossings within the first year of the tour until day 200 in 2005. The dust impact rates shown are based on the DA counter data. The counter criteria are quite complicated and their description is beyond the scope of this paper. The criteria include the evaluation of the signal amplitudes, risetimes, integrals, baseline heights, number of peaks (multiplier channel only) and the amplitude ratios between the channels.[2]

The figures in this section (Figs. 4–16) showing the impact rates are composed of three sections, the upper two giving trajectory and pointing information, with the dust impact rates onto the DA at the bottom.

[2]Ratios between the ion grid channel and the target channels are important to decide between an impact onto the small chemical analyser target and the big ionisation detector target (Srama et al., 2004).

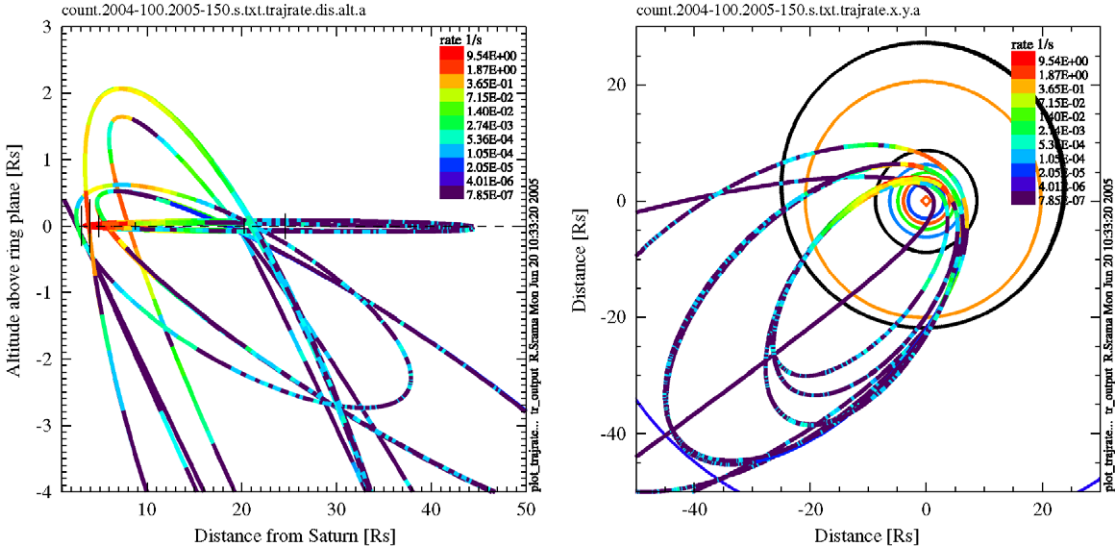

Fig. 3. The Cassini trajectory plotted with colours representing the CDA dust impact rate. The event rate is highly fragmented due to changes of the Cassini spacecraft attitude. The event rates rise with decreasing distance to Saturn. The moon orbits are shown in: black (slightly eccentric orbit of Hyperion), orange (Titan), Rhea (black), Dione (blue), Tethys (green) and Enceladus (red).

The upper section of each figure shows the angle in degrees between the CDA boresight and the ring plane. A positive angle is defined such that CDA points upwards into the northern hemisphere. Zero corresponds to the CDA boresight parallel to the ring plane. The blue curve shows the distance of Cassini to the ring plane (with the y-axis scale as distance in 1000 km).

The middle section shows the angle between the CDA boresight and the dust RAM direction. For this calculation we assume circular prograde dust orbits. Above an angle of 50, no particles on circular prograde orbits can hit the impact target of DA. However, impacts on the inner wall of DA might be detected up to impact angles of almost 90 (note the central CAT has an aperture with a half-cone angle of 28, compare Srama et al., 2004). An angle of zero corresponds to a normal incident direction.

The bottom section shows the overall DA event rate (black curve) and the impact rates with small impact charges (blue) and big impact charges (red). Vertical bright blue stripes mark times when the DA was not in a measurement configuration (mainly caused by articulations with a duration of 15–30 min). During the activation of the articulation platform the event definition has to be switched off and no events can be recorded.

The impact rates are based on two different classification schemes. The FSW before version 10.0 used 20 counters and processed the data until DOY 150 in 2005. The three rate curves are: red representing class 3 events including the counters 2, 3, 6, 7, 8, 9, 14 and 15. This class covers highly reliable dust impacts with amplitudes well above the noise level and a mass threshold of approximately 5.0×10^{-15} kg (the mass threshold is velocity dependent and here we assume an impact speed of 7.5 km s^{-1}; ice particle with 2.1 μm diameter); blue covering the counters 10, 11, 12, 13, 17 and 18, which represent the class 2 events (mass threshold of 1.0×10^{-16} kg or ice grains with a diameter of 0.55 μm). Ninety to Ninety-five per cent of these events are believed to be true dust impacts with moderate amplitudes; black includes all counters (including the noise counters 16 and 19)[3] and shows the highest rate.

Impact events represented by the counters of the red curve are called hereinafter big particle impacts and the events related to the blue curve are called small particle impact. However, the detection thresholds of the counters react to impact charges and the particle speed has a dominant influence on the impact charge. The separation between big and small impacts becomes true by considering an almost constant impact speed.

The rates shown after DOY 150 of 2005 (Figs. 14–16) are based on the classification and onboard processing with FSW version 10.0. Here, we define the red curves as the sum of class 2 and class 3 events, which are almost 100% true dust impacts with a mass threshold of 5.0×10^{-15} kg. As defined in Table 6, class 3 events describe strong impacts and cover the counters 0, 2, 8, 9 and 11, whereas class 2 events are used for medium sized dust impact charges and include the counters 1, 3, 10, 12 and 7. The blue curve includes the counters 4, 5, 6, 17 and 18 of class 1, which count small dust impacts on the IID or the CAT with a mass threshold of 3.5×10^{-16} kg (ice grain of 0.87 μm). Even class 1 events are more than 90% real impacts, due to a reliable onboard evaluation scheme. The noise and low-quality counters are 13, 14, 16, 19, 20, 21, 22 and 23 and they correspond to class 0, but even these counters include many real dust impacts like dust stream

[3]Not included are the counter 0, 1 and 4 which represent test pulses and the internal interrupt loss counter.

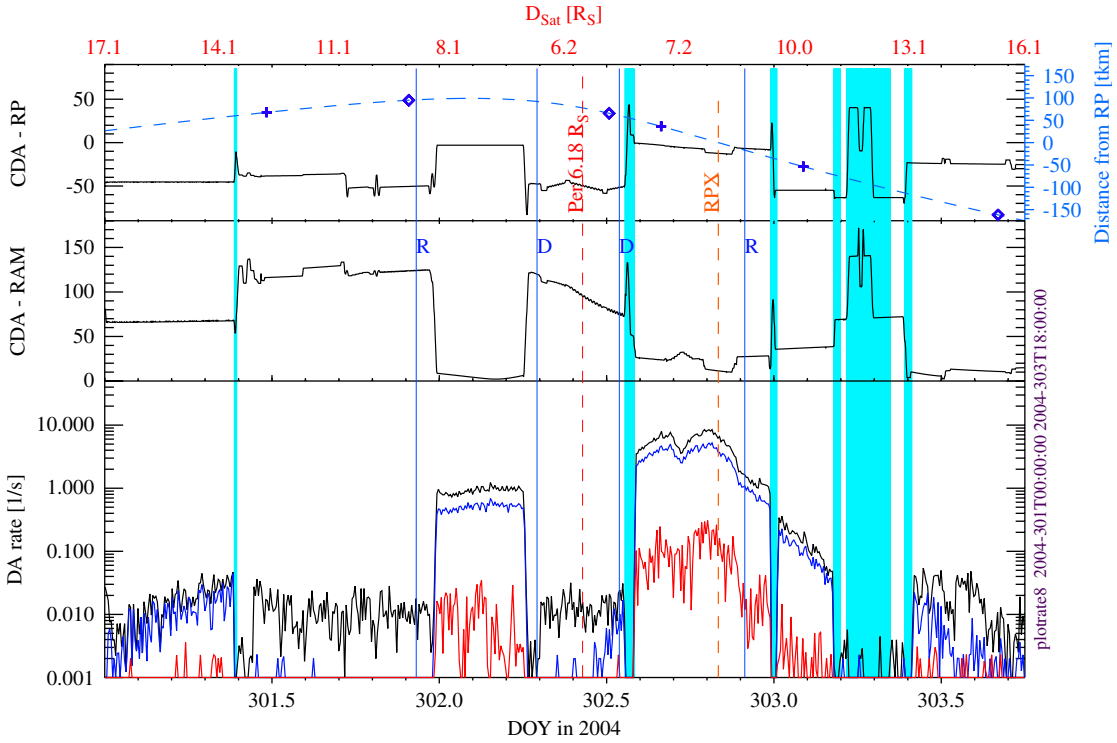

Fig. 4. Pointing geometry and dust impact rates for the first inner ring plane crossing of Cassini at Saturn (orbit a). The top panel shows the angle in degrees between the CDA boresight and the ring plane (black line) as well as the distance of Cassini from the ring plane in units of 1000 km (dashed blue line). The symbols on the dashed line indicate crossings of different latitudes (cross: 5°, diamond: 10°, triangle: 15°, square: 20°). The middle panel shows the angle between the CDA boresight and the dust RAM direction assuming circular prograde orbits. The lower panel shows impact rates based on classification before software version 10: red line is class 3 events, blue line is class 2 events and black line all events (see text for details). The red numbers at the top are Cassinis distance from Saturn in units of R_s. The red line labelled 'PER' indicates the time of periapsis and the dashed red line labelled 'RPX' indicates the time of ring plane crossing. The lines labelled R, D, T, E and M indicate the time of crossings of the orbits of the moons Rhea, Dione, Tethys, Enceladus and Mimas, respectively. The vertical bright blue bars indicate the time periods where CDA was not in a nominal measurement configuration (CDA did articulate, CDA was off or in a standby mode).

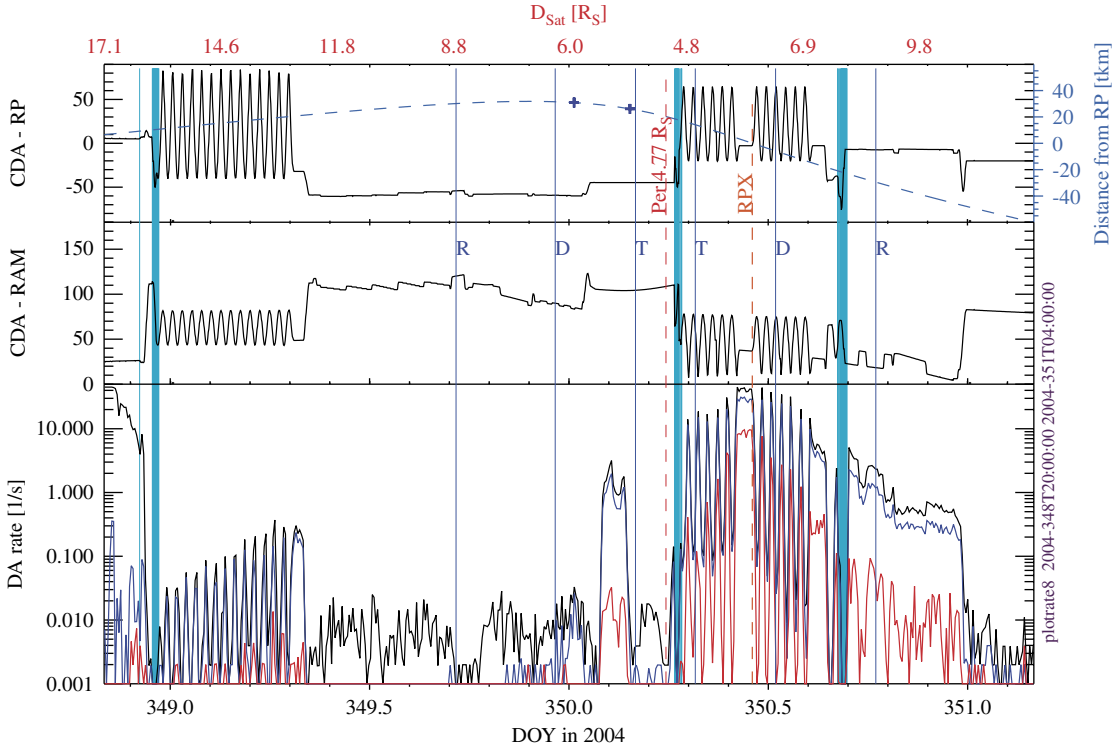

Fig. 5. CDA pointing and dust impact rates at the inner ring plane crossing on orbit b.

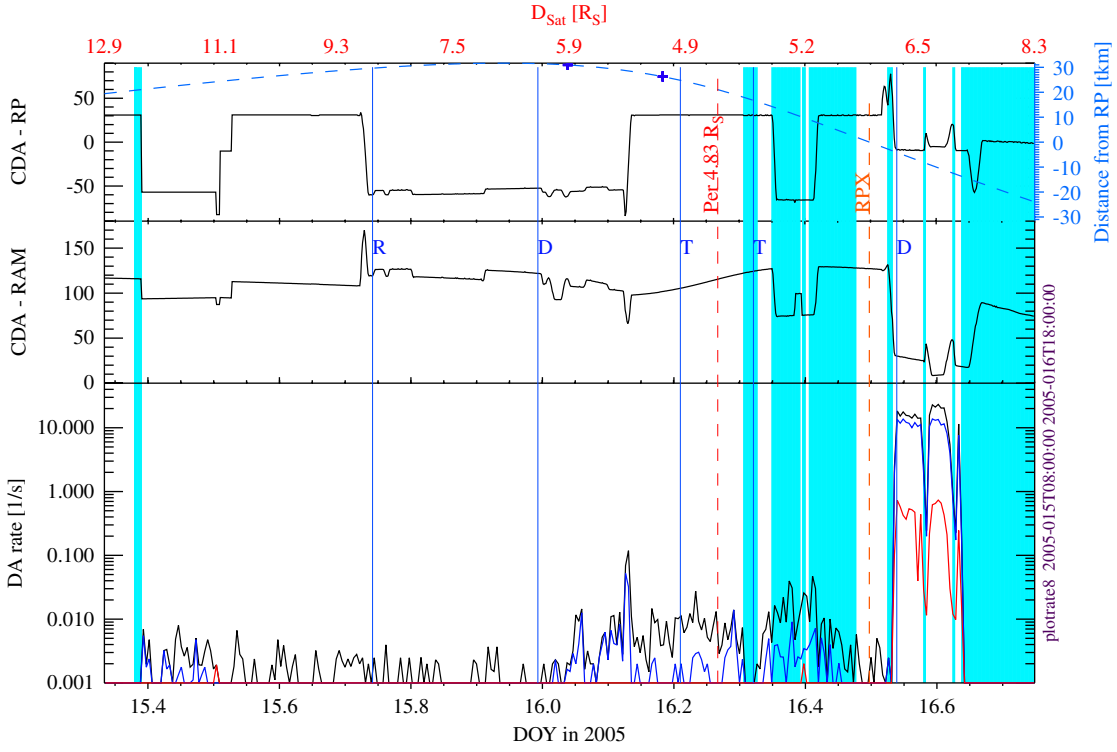

Fig. 6. CDA pointing and dust impact rates at the inner ring plane crossing on orbit c.

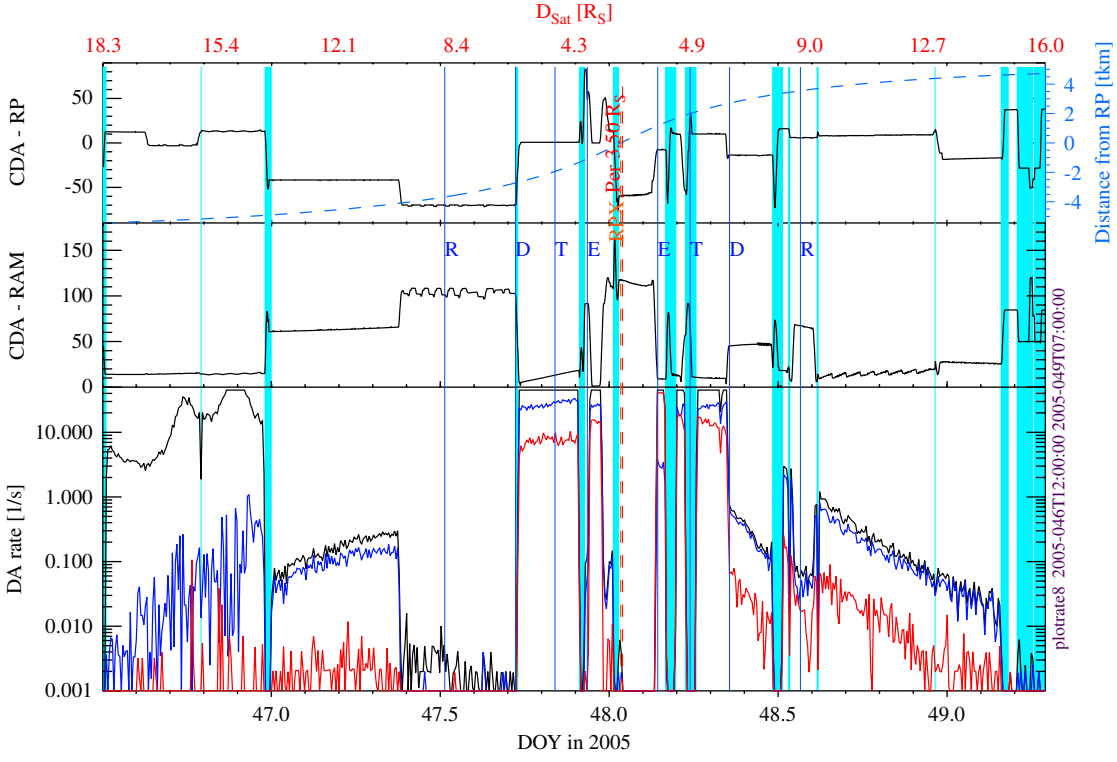

Fig. 7. CDA pointing and dust impact rates at the inner ring plane crossing on orbit 3.

particles with low-impact charges or impacts on the inner wall or struts of the DA aperture. The ratio of real impacts to noise (plasma fluctuations, sounder events, mechanical noise and disturbances on the electrical ground) is highly variable but can reach values of more than 50% of real impacts during ring plane crossings. The black curve shows

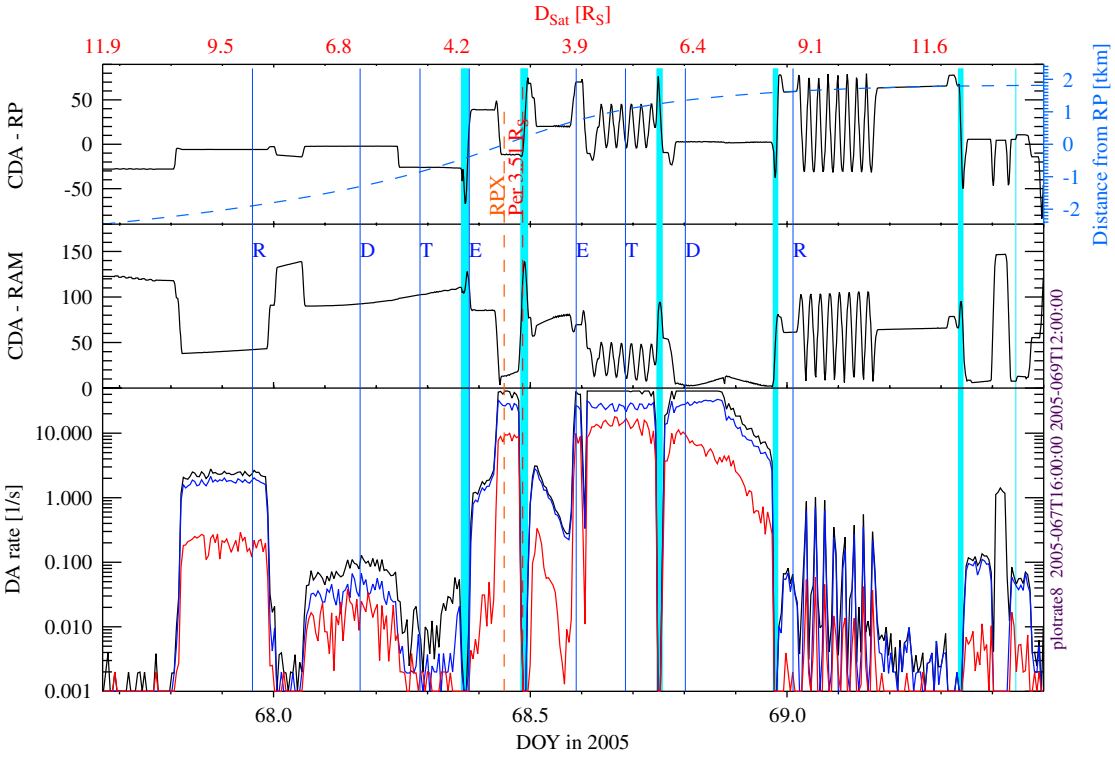

Fig. 8. CDA pointing and dust impact rates at the inner ring plane crossing on orbit 4.

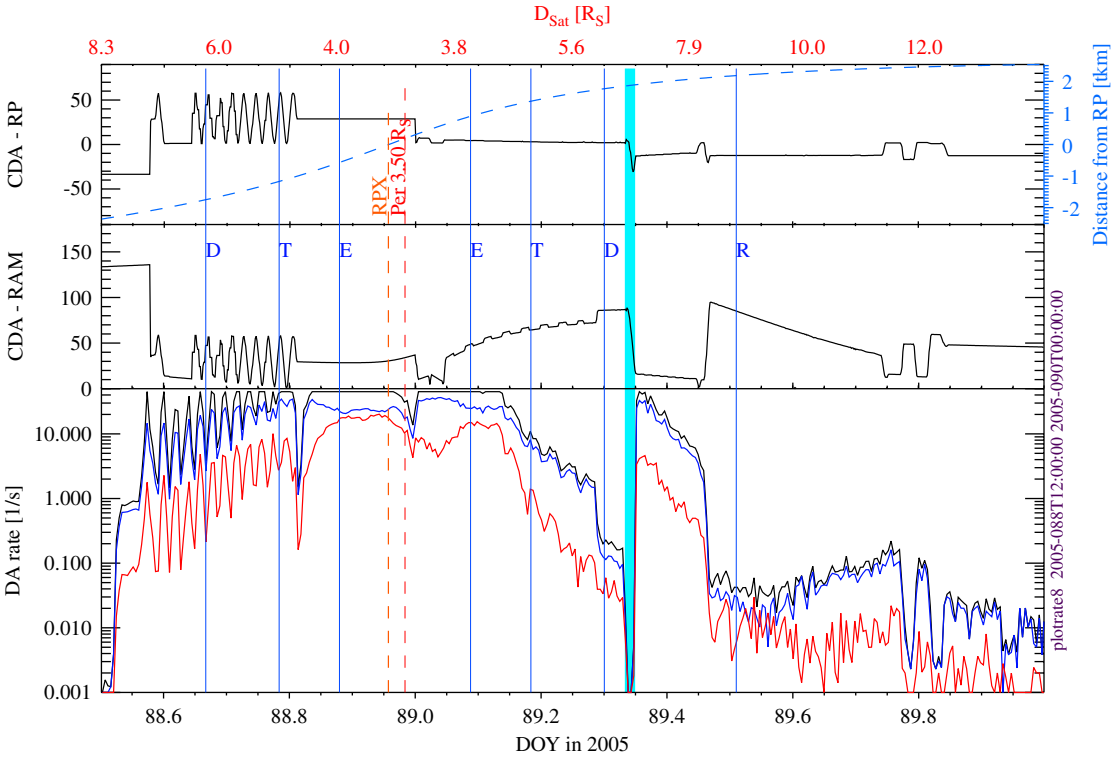

Fig. 9. CDA pointing and dust impact rates at the inner ring plane crossing on orbit 5. The stable pointing angles around DOY 88.6 is caused by CDA data gaps and the changes of the boresight were not reconstructed.

the highest rate and is composed of the sum of class 0, class 1 class 2 and class 3. These rate definitions allow for a good comparison of the rate plots before and after DOY 150.

We now discuss the dust rates obtained during each inner ring plane crossing. The first ring plane crossing data were obtained around DOY 2004-302 and the

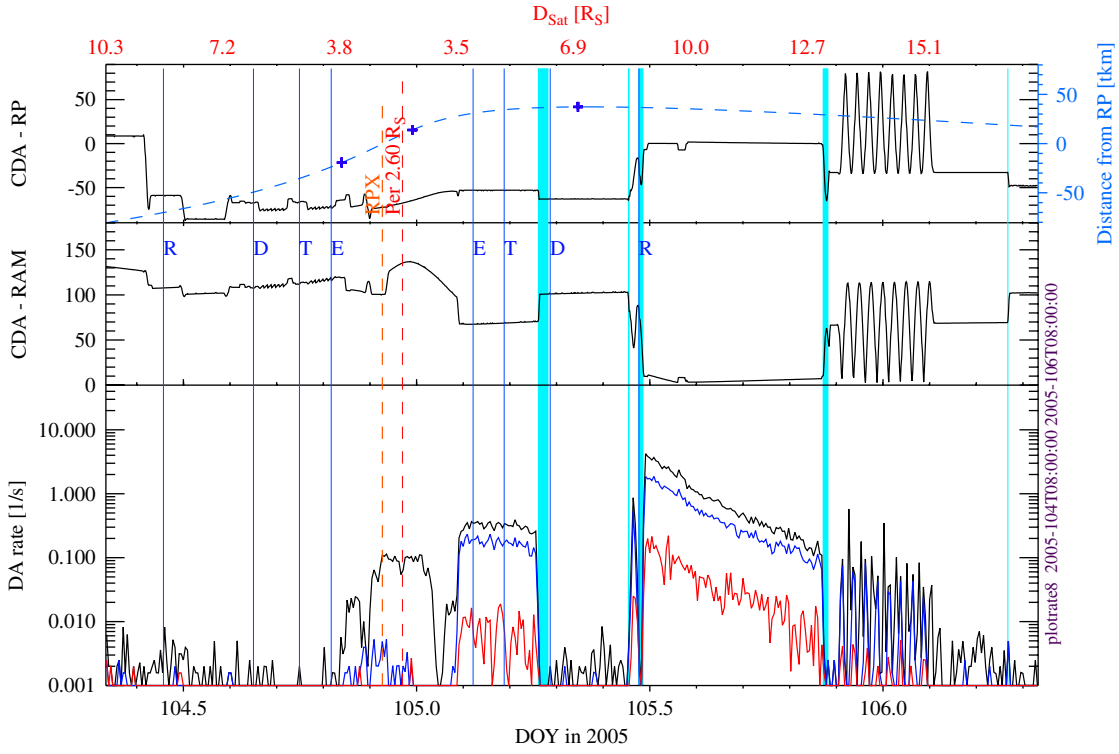

Fig. 10. CDA pointing and dust impact rates at the inner ring plane crossing on orbit 6.

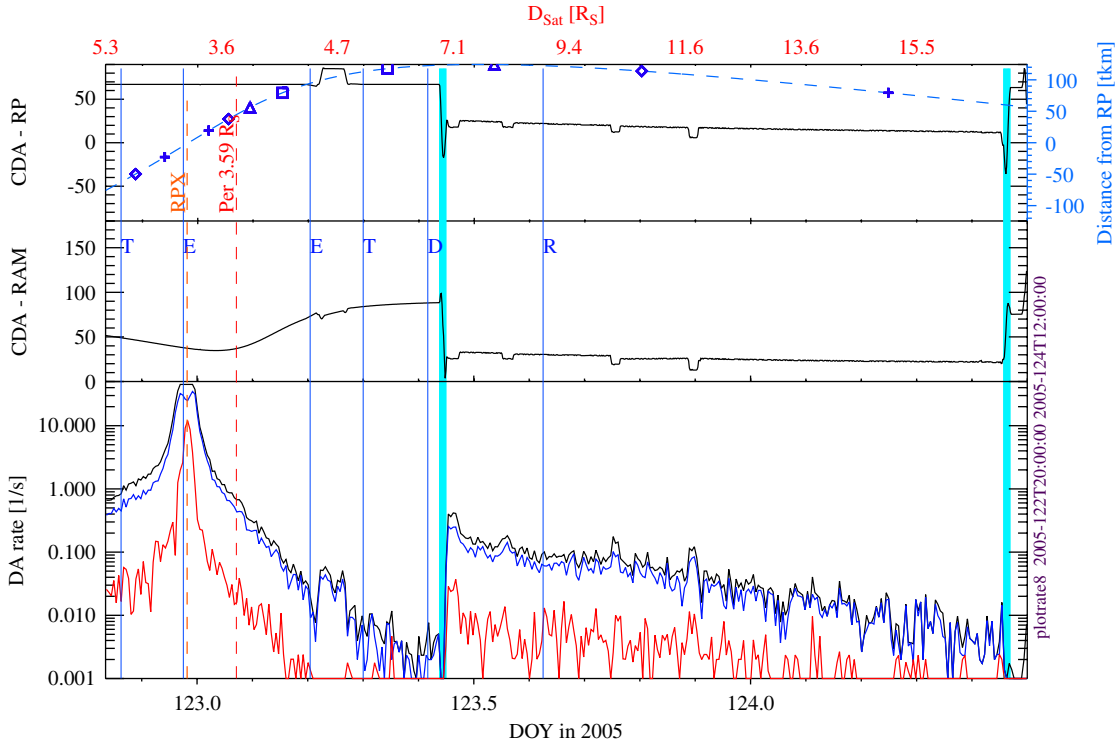

Fig. 11. CDA pointing and dust impact rates at the inner ring plane crossing on orbit 7.

corresponding rate profiles are shown in Fig. 4. At 2004-302T04:17 Cassini reached a Saturn distance of 7.0 Saturn radii (R_s) and a latitude of 13.5 which corresponds to an altitude of 100 000 km. Periapsis occurred at 6.18R_s and the ring plane crossing occurred at DOY 302T20 at a distance of 8.0R_s. For the first time, DA measured dust at high

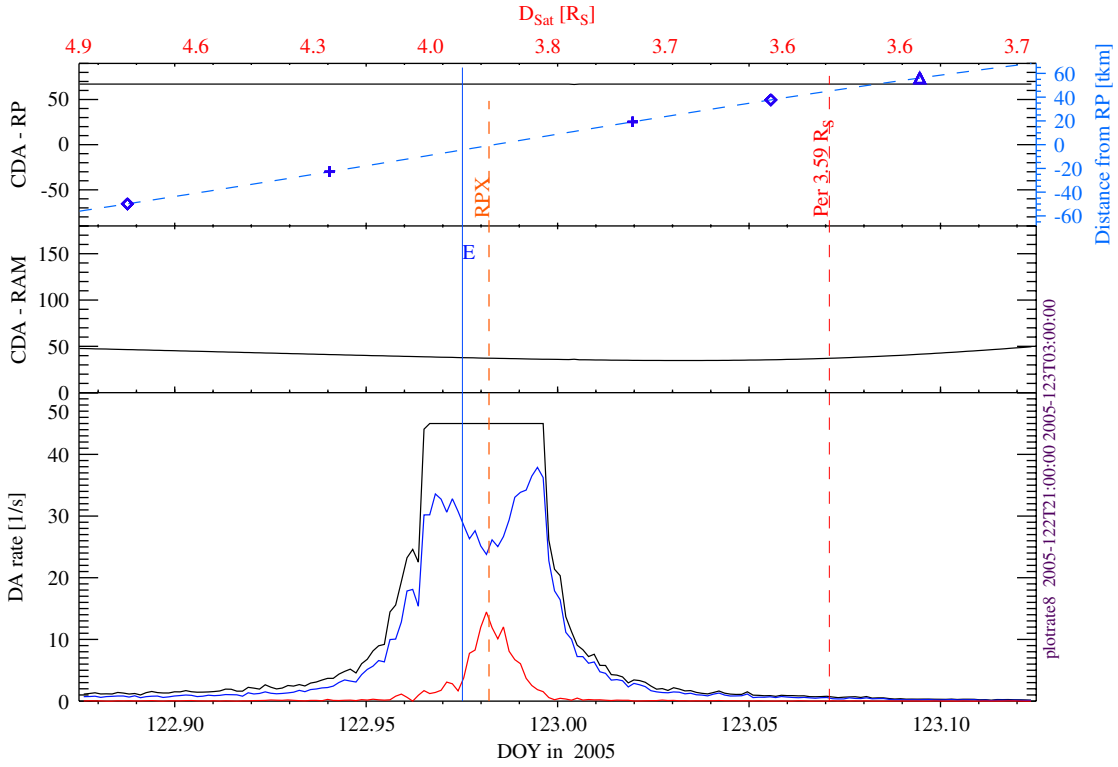

Fig. 12. The DA impact rate of the ring plane crossing of orbit 7 with a higher time resolution.

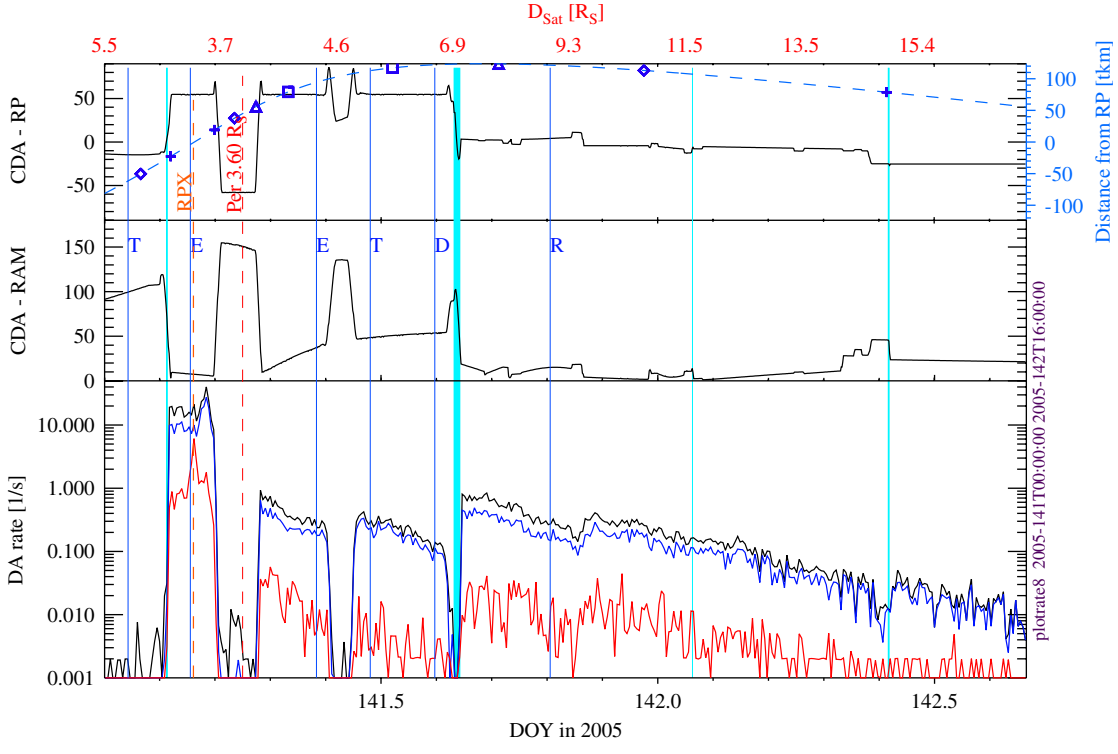

Fig. 13. CDA pointing and dust impact rates at the inner ring plane crossing on orbit 8.

altitudes as far as 100 000 km above the ring plane (early on DOY 2004-302). Beyond distances of $10R_s$ the impact rate is still significant (early on DOY 303). The onset of dust impacts occurred at a distance of $17R_s$ and altitude above 20 000 km at the beginning of DOY 2004-301. After an unfavourable pointing geometry during the second half of

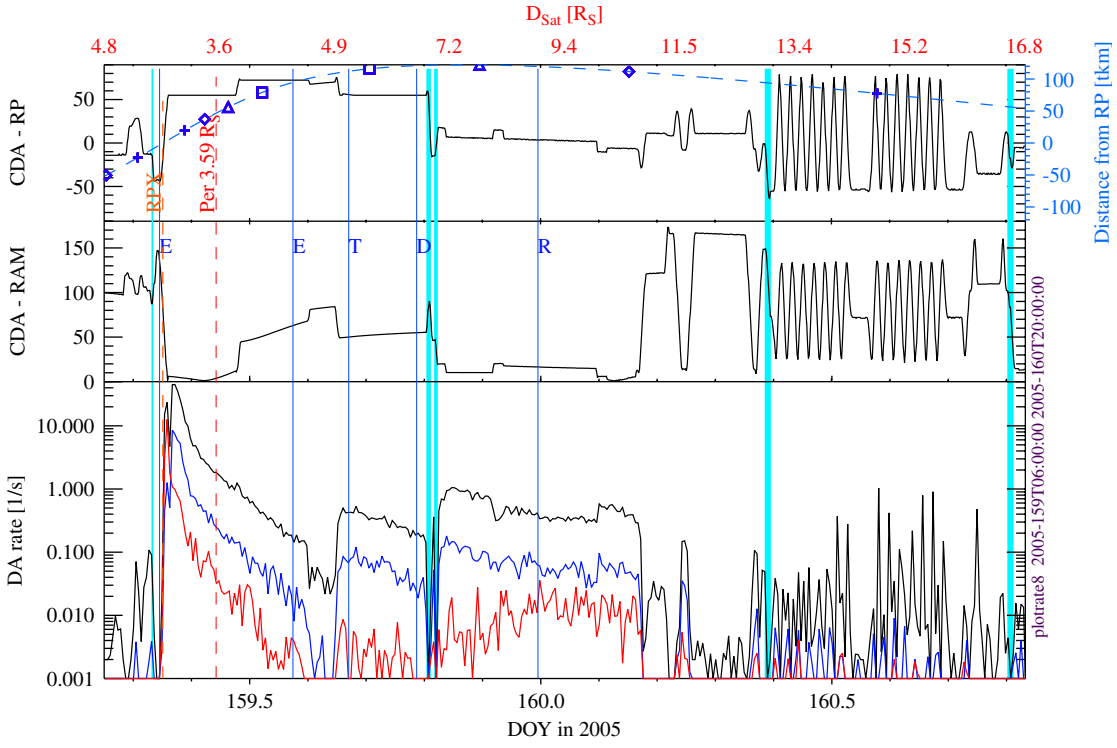

Fig. 14. CDA pointing and dust impact rates at the inner ring plane crossing on orbit 9.

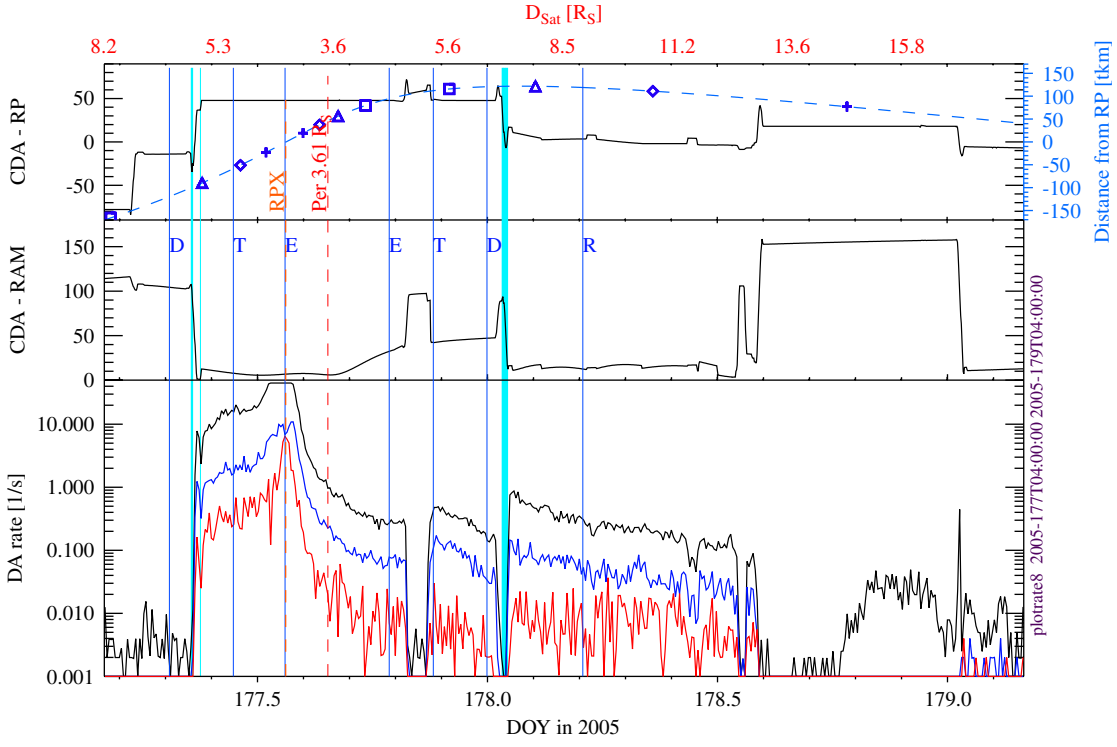

Fig. 15. CDA pointing and dust impact rates at the inner ring plane crossing on orbit 10.

DOY 301, DA registered clear dust signals between 8 and 6.5R_s at altitudes of 100 000 km with an impact rate of approximately 1 s^{-1}. The impact rate increased with approach to Saturn and at lower altitudes (DOY 302). Between 8 and 9R_s distance, the impact rate was still very high and close to the saturation limit of the instrument

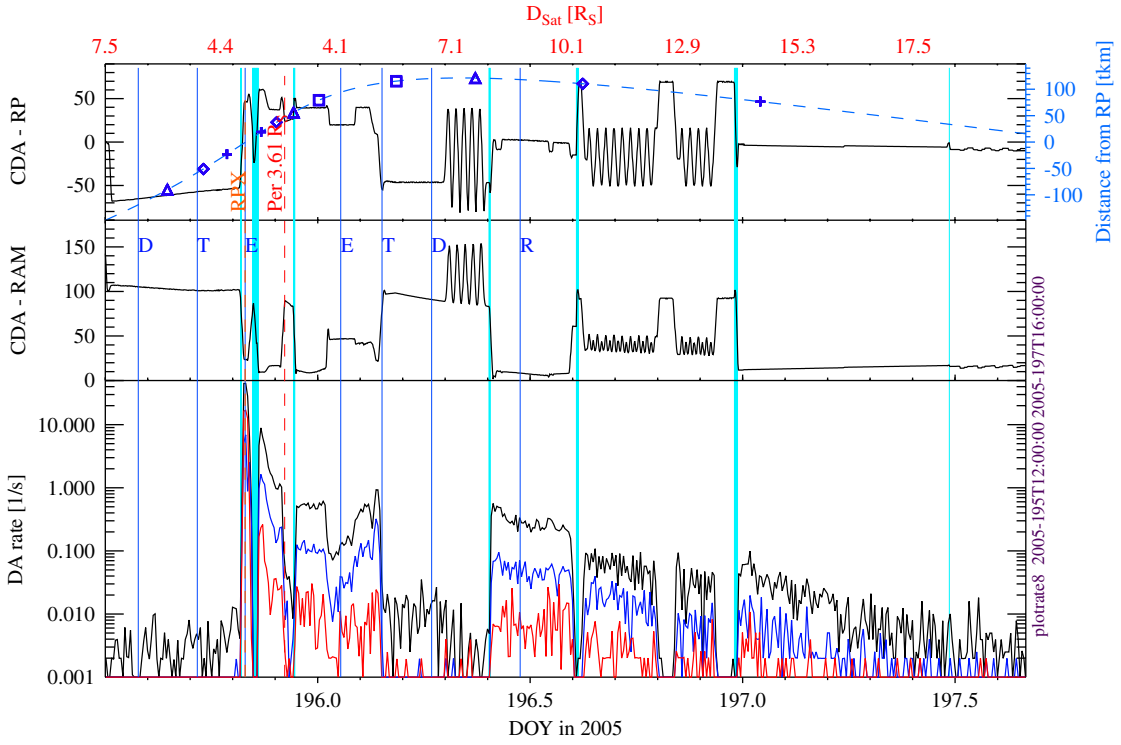

Fig. 16. CDA pointing and dust impact rates at the inner ring plane crossing on orbit 11.

(1 s dead time). The rates are dead time corrected and therefore show values above 1 s^{-1}.

The measurement geometry was different for the second ring plane crossing around DOY 2004-350 (Fig. 5). The rolling downlinks during which the CDA-ring plane angle changed significantly (DOY 349 and DOY 350) are very obvious. The second roll was interrupted due to Cassini internal flight rules. During this part of the orbit Cassini stayed within a distance of 30 000 km of the ring plane except at the end of this segment when it finally reached a distance of 60 000 km. The rolls led to strong variations of the dust impact rates. This can be observed at low dust densities further out (around 15R_s), as well as within 7R_s. Nevertheless, the envelope of the rate maxima during rolls still follows a clear trend; it rises during the approach phase on DOY 349 and increases and decreases before and after the ring plane crossing on DOY 350. As soon as the CDA boresight angle to the dust RAM direction exceeds approximately 60, the impact rate falls by orders of magnitude (DOY 351T00). On its outgoing pass, DA observed significant impact rates beyond 10R_s (between 0.2 and 0.5 s^{-1}).

The correlation between the CDA pointing and the observed impact rate was confirmed during the ring plane crossing around DOY 2005-016. Fig. 6 shows almost no dust impacts until DOY 16 when the pointing improved and some wall impacts were registered. After the Dione orbit crossing (DOY 16.5) the boresight pointed close to the dust RAM direction and the dust rates rose immediately to saturated values. Altogether, this orbit had a very bad geometry for CDA and no major results were achieved.

The geometry changed significantly in orbit 3 with its targeted Enceladus encounter at 2005-048T03:30 and a flyby altitude of 1260 km. Furthermore, Fig. 7 shows that this orbit had a low inclination and Cassini remained close to the ring plane for the entire time. This would have been optimal for investigations of dust densities during satellite orbit crossings. However, many pointing changes occurred close to the moons orbital distances and no significant variations of dust impact rates during the orbit crossings could be observed. Close to the periapsis and ring plane crossing the spacecraft went into a safe attitude with the high-gain antenna pointing towards dust RAM (in order to protect the subsystems from big dust impacts). This orbit segment shows quite a number of interesting features. First, the approach phase showed a high number of impacts (ring particles and stream particles) between 16 and 10R_s. Due to the marginal pointing, small impacts (i.e. low signals) dominated with a low rate of big particle impacts. Within 6.3R_s the instrument was saturated, but a decrease of dust impacts was observed on the outgoing pass outside 6.3R_s. Therefore, DA could not resolve a dust impact rate profile during the Enceladus encounter. However, the HRD instrument showed dust flux variations which were high at the orbit of Enceladus. These results will be reported elsewhere. Fortunately, the observing geometry was stable and convenient outside 10R_s and a decrease of the impact rate of 1 s^{-1} at 10R_s down to 0.1 s^{-1} at 15R_s was detected.

Fig. 8 shows the dust rate observed in orbit 4 within approximately $11R_s$ around periapsis. Outside this range the measurement conditions were not favourable for CDA. The following observations were made: First, a constant rate of about $1\,s^{-1}$ was detected during approach around $10R_s$. This rate is slightly higher than during the previous observations and might be caused by the low elevation above the ring plane and by a significant contribution from stream particles.[4] Second, a rocking downlink was performed starting at 068T14:46. This rocking modulated the impact rate although the instrument was saturated. At approximately $7R_s$ distance the impact rate decreased followed by a modulation of a rolling downlink around the beginning of DOY 69. The rates of the outgoing part correspond to the rates of the day 2005-048 (approx. $1\,s^{-1}$ at $10R_s$). Finally, measurements at 69T11:00 provided rather high rates up to $0.5\,s^{-1}$ at $13R_s$.

A second rocking downlink was performed on day 2005-088 leading to impact variations of two orders of magnitude (Fig. 9). The instrument was in saturation again in the inner Saturnian system. The first rate variations were observed on the outgoing part of the trajectory starting at $4.5R_s$. On the other hand, the boresight was approximately 50 away from the dust RAM direction which limited the observable number of particles. CDA had good pointing for dust measurements for only a short period before noon on DOY 89. The rate measurements around $8R_s$ still have values of $3\,s^{-1}$ and confirm the high rates monitored in previous orbits. More interesting is the phase between 10 and $12R_s$ showing an increasing dust flux with increasing distance from Saturn. This is caused by changes of the geometry: the CDA boresight went closer to the dust RAM direction leading to a larger sensitive area for circular prograde particles.

Cassini often observes Saturn with its optical remote sensing instruments. These instruments point into the $-y$ direction which is almost the opposite direction to the CDA mounting axis onboard Cassini. On the other hand, the dust RAM direction is located on the leading side of Cassini as long as Cassini is orbiting faster than the dust particles.[5] During the ingoing part (before periapsis) of Cassini's trajectory, dust measurements are therefore excluded while the cameras point towards Saturn. This occurred for a long time in orbit 6. The ingoing part had a bad viewing geometry for dust measurements (Fig. 10). This changed on the outgoing part where DA observed a clear decrease of the dust impact rate with distance from Saturn. The pointing was stable and optimal between 9.5 and $13R_s$. This observation was followed by a downlink roll which modulated DAs impact rate accordingly. A significant dust flux remained and was monitored until $15R_s$ where an impact rate of $0.1\,s^{-1}$ was detected.

The following ring plane crossing in orbit 7 had only a few major changes in spacecraft attitude. This allowed rather smooth rate measurements between $5R_s$ on the ingoing part and $17R_s$ on the outgoing part. Minor changes in the spacecraft pointing are reflected in small increases of the impact rate (123T12:00–124T00:00). On the other hand, this orbit had a higher inclination and therefore big elevations above or below the ring plane. The result of the impact rate measurements is shown in Fig. 11. The peak impact rate of small impact charges shows a small slump at the ring plane crossing at 122T23:36 (Fig. 12). This causes two maxima before and after the ring plane crossing separated by approximately 35 min. In this time the spacecraft moved from about -2 latitude to $+0.8$ latitude. The relation between small (dark blue curve) and big impact charges (red curve) are anti-correlated at the time of the ring plane crossing (122T23:36). However, the measurement geometry was very stable leading to the conclusion that the dust population changes with distance from the ring plane. The profile is reminiscent of the shape of Jupiters Gossamer ring where the vertical ring extention is related to the inclination of the moons (Ockert-Bell et al., 1999). Here, the only moons with an inclination above 1 are Tethys and Mimas. The relative impact velocity for circular prograde particles was $8\,km\,s^{-1}$. Later measurements on day 2005-177 showed a similar counter profile (not shown in this paper).

The quick rise of Cassini elevation above the ring plane was accompanied by a fast decrease of the impact rate. Changes of the CDA angle towards the ring plane in mid DOY 123 (Dione orbit crossing) led to dust detections at elevations above the ring plane as far as 120 000 km (at $7R_s$, 17 latitude). This was followed by only a gradual decrease in the impact rate with distance from Saturn. However, one has to take into account that Cassini came closer to the ring plane with increasing distance. Although only minor pointing changes occurred, due to the high ring plane elevations, this data set is again not suited for an analysis of dust densities around satellite orbit crossings. Some impact rates based on this data set are listed in Table 7.

The data around periapsis of orbit 8 are shown in Fig. 13. This data set is rather similar to that of orbit 7. Within $7R_s$ more pointing changes occurred and the rate profile was more fragmented. On the other hand, the measurements were better in places than in the previous orbit. Starting at $7R_s$ on the outgoing segment, continuous coverage of the ring was possible until $17R_s$ However,

Table 7
Impact rates derived from the data set on DOY 2005-123

DA impact rate (s^{-1})	Distance from Saturn (R_s)	Elevation above ring plane
1	5	−50 000 km
1	3.6	+40 000 km
0.2	7	+120 000 km (17 latitude)
0.01	14	+75 000 km

[4]Stream particles are identified in the raw data of impact signals.

[5]This effect is similar to that of snow flakes observed from within a fast car. The snow appears from ahead rather than from above.

during the scan the elevation to the ring plane changed again significantly. It fell from 120 000 km at $7R_s$ down to 55 000 km at $17R_s$. Once again high impact rates of dust particles were observed by DA at high altitudes above the ring plane. The rate observed was $0.3\,s^{-1}$ at a distance of $10R_s$ and an elevation of 100 000 km. An inspection of the raw data revealed reliable dust impacts with impact speeds between 7 and 40 km s^{-1}.

The entire ingoing pass on orbit 9 was lost due to unfavourable measurement geometries. Therefore, the plots in Fig. 14 start at 159T08:00 with the onset of the high impact rates. The outgoing pass had many changes in spacecraft attitude and a rolling downlink on DOY 160. An inspection of raw impact signal data showed evidence for water ice particles at elevations of 50 000 km and above (at $\sim 4R_s$). Furthermore, the rate between the Tethys and Dione orbit crossings is based on real impacts, although the CDA boresight was neither in the ring plane nor close to the circular RAM direction. At $7.8R_s$ further water ice particles were identified at latitudes of 15.

An asymmetry of the impact rate before and after the ring plane crossing at 2005-177T13:30 was observed on the incoming part of orbit 10 (Fig. 15). The spacecraft pointing was stable and cannot be the reason for this change. The relative impact speed of the particles onto the detector or an asymmetry of the vertical dust density profile can influence the observed rates. Before the ring plane crossing, the impact speeds were higher and the relative impact speed was continuously decreasing. At 177T11:00 the relative impact speed of circular prograde particles was 8.6 km s^{-1} and at 177T16:00 the speed was 6.5 km s^{-1}. More details are discussed in Section 5.

In general, the geometry of orbit 10 is similar to conditions of orbit 9. The ring plane crossing occurred at the orbit of Enceladus and the orbit has a slight inclination. A scan of the dust population was possible between $6R_s$ of the ingoing segment until $13R_s$ of the outgoing part. Continuous dust measurements under exceptionally good conditions occurred between 7 and $13R_s$ Some impact rates achieved at this orbit were: $>0.02\,s^{-1}$ ($5.6R_s$, 80 000 km below the ring plane), $0.1\,s^{-1}$ ($4.3R_s$, 100 000 km above the ring plane) and $\sim 0.1\,s^{-1}$ ($11R_s$, 100 000 km above the ring plane). The rates given at 5.6 and $4.3R_s$ were measured with a CDA boresight pointing 50 above the plane. This decreased the sensitivity for low-inclination circular particles significantly and this has to be corrected. The true impact rate under optimal conditions would probably have been much higher.

The last ring plane crossing considered in this paper occurred on DOY 195 (Fig. 16). This orbit showed the typical low sensitivity for dust measurements during the approach phase due to the unfavourable spacecraft attitude. At 195T19:55 a targeted flyby of Enceladus occurred with good pointing for dust measurements. This flyby occurred at an altitude of 172 km and the flyby data showed a strong enhancement of dust particles right before closest approach. A comparison with models identified the south polar region of Enceladus as a main dust source of E ring particles. Further details are reported in Spahn et al. (2006). Beyond the Enceladus campaign, the attitude changes of Cassini did not allow useful measurements in the inner Saturnian system. At $8R_s$ the geometry changed and CDA performed a further scan of the outer environment up to distances of $15.5R_s$. This phase included a rocking downlink on DOY 196. The rock can be recognised by a scan of a smaller angular range which corresponds to the small modulation of the CDA boresight towards the dust RAM direction. DA detected reliable dust impacts at large distances and high latitudes above the ring plane (similar to the results from orbit 10), in the time frame between 196T10:00 and 197T04:00.

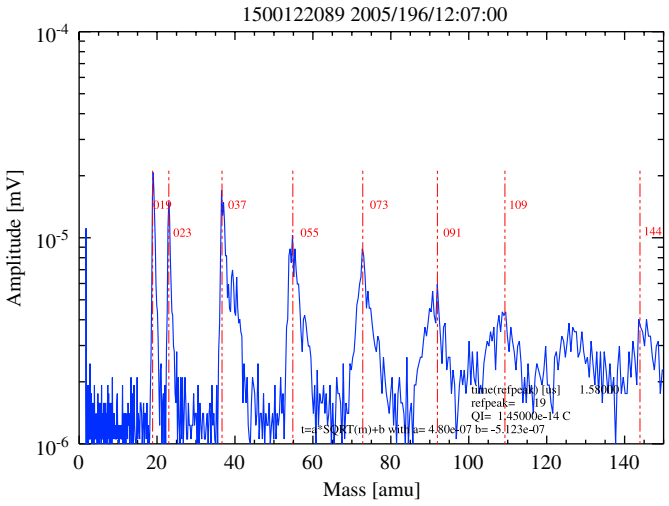

Fig. 17. Time-of-flight mass spectrum of a dust particle impact on DOY 196. The peak pattern is caused by clustering of water molecules. The strong line at 19 amu represents the hydronium ion (H_3O^+) and the consecutive peaks with the masses 37, 55, 73, 91 and 109 are attributed to attached water molecules ($H_3O^+(H_2O)_x$).

An example of a mass spectrum recorded during this time segment is shown in Fig. 17.

5. Discussion

The data presented have clearly shown a wide distribution of dust particles around Saturn. The first indication of high-altitude dust was measured in the year 2004 on DOY 302 (October 28) at elevations as high as 100 000 km above the ring plane at distances of $7R_s$ from Saturn. The derived dust densities for particles bigger than 0.5 μm is rather high and reaches values as high as $0.001\,m^{-3}$. These results confirm the discovery of dust particles outside the ring-plane measured by the plasma wave instrument onboard Voyager 20 years ago (Gurnett et al., 1983).

The dust densities ρ can be derived from the sum n_r of the red and blue curve of the impact rate (s^{-1}) and the relative dust impact speed v ($m\,s^{-1}$) simply by $\rho = n_r/A \times v$.

High dust densities[6] at high latitudes are a surprising new result and there is no doubt that the corresponding counter events are related to real dust impacts. This conclusion is supported by the analysis of individual raw impact signals. Normally, the DA instrument provides raw data of impact signals with an efficiency between 1% and 100%. The remaining data are either transferred with their processed information (amplitudes, risetimes, integrals) or they are classified and increment one of the counters. Many counters classify reliable impacts such that the impact rates can be derived from this information only if necessary. Only long data gaps of CDA housekeeping packets make a rate analysis difficult. Long gaps are defined as the time between two counter overflows. An unrecognised counter overflow would corrupt the rate information. On the other hand, high impact rates above $1\,s^{-1}$ have to be derived using a dead time correction. This causes further uncertainties with rising rates. Here, we limit the rates plotted to a maximum of $45\,s^{-1}$. More accurate rate information can only be given with better knowledge of the accumulated dead time. The dead time after an individual impact is on average 1 s with an uncertainty of 125 ms. New FSW with more accurate dead time information is in preparation. This will allow the reliable derivation of impact rates above $10\,s^{-1}$ up to approximately $100\,s^{-1}$.

Not shown in this paper are mass distributions and impact velocity distributions. For a derivation of those properties a more detailed analysis of the raw impact signals is necessary and this will be published elsewhere.[7] Furthermore, the impact rates are dominated by Saturn stream particles at larger distances. The exact contribution of stream particles to the data set presented is not yet determined. However, it is clear that the dust found at high latitudes and distances between 8 and $15R_s$ cannot belong to stream particles alone. This conclusion is derived from a sporadic investigation of the raw data set.

Where does the dust at high latitudes come from? Do the particles belong to the halo population as predicted by models of Howard et al. (2000)? This question cannot be clearly answered. The dynamical properties of halo dust particles are not clearly separated from non-halo particles which would allow a clear distinction in the data set. Although a detection of halo particles cannot be confirmed, it can also not be excluded.

What are the particles at high latitudes made of? Are there compositional variations of particles within the E ring and the extended dust environment? This question was not addressed in this paper but CDA was able to record and deliver the data necessary to answer this question to the ground. An analysis of this topic is therefore ongoing. However, it can be stated that water ice particles were found in the entire dust environment, at high and low latitudes and at all distances from Saturn within $15R_s$. The mass spectra of water ice particles with impact speeds of approximately $10\,km\,s^{-1}$ are very characteristic with their repetitive peaks of water molecule clusters. Such features were recognised in the spectra of the majority of the micron sized grains which provided a time-of-flight mass spectrum. Furthermore, silicate features were identified in some spectra (Hillier et al., 2006).

The strong variations of the DA impact rate with the boresight angle towards the dust RAM direction show that the impact rates are dominated by prograde Keplerian particles. A separate retrograde dust population has not been identified in the data set so far. The predicted dust densities of retrograde particles are very low ($10^{-9}\,m^{-3}$) and its detection in the inner Saturnian system would still be difficult due to the high noise and particle background. Three-dimensional simulations predict a tenuous ring of captured interplanetary particles into retrograde orbits (Mitchell et al., 2005). This dust, which has a typical size of 0.1 μm, forms a thick ring around the planet between the main rings and 9 planetary radii with a thickness of approximately 3 planetary radii. However, due to the very low density, only 20 retrograde grains would be detected by DA during the first four years of the Cassini mission.

The overall amount of dust within Titan's orbit was very surprising. The questions that are immediately raised are: Do these particles belong to one big, faint ring and extend the E ring which was defined between 3 and $9R_s$ earlier in the literature? Are there gaps or short scale density gradients in the extended dust environment? Are there dust density enhancements or different dust mass distributions along satellite orbits? The answer to such questions is not obvious and cannot be given without a more detailed data analysis. A jump in dust density during orbit crossings of Enceladus, Tethys, Dione and Rhea was not identified in the DA data set so far. Such variations are difficult to detect in the inner ring due to the saturation of the DA instrument which makes a rate analysis impossible within $6R_s$. However, the mass distribution is still reflected in the DA data set and there are indications for big particles along Enceladus orbit. The analysis of the HRD measurements will help to understand the distribution of particles above 2 μm in the inner E ring.

For a determination of the real dust densities within the E ring and its extended region, some further processing of the dust rates is necessary. The geometric sensitive area of DA towards the dust RAM direction and the relative impact speeds have to be taken into account. Furthermore, the DA detection threshold varies with impact speed. For rising impact speeds, smaller particles are detected. The impact rate depends on the density of tiny particles which are smaller than e.g. 0.5 μm. Slight increase of the spacecraft speed (or more correctly the relative dust impact speed) will cause significantly higher fluxes if the dust environment is dominated by tiny ($<0.5\,\mu m$) grains (compare Eq. (1)). One good example is the rate observed

[6]The recorded impact speeds varied between 5 and $>50\,km\,s^{-1}$. Therefore, grains on bound and unbound orbits were detected. The relative impact speed of circular prograde particles on day 2005-123T11:00 onto CDA was $8.4\,km\,s^{-1}$.

[7]A coarse investigation of the data set shows mainly impact speeds between 8 and $30\,km\,s^{-1}$ within $12R_s$.

in orbit 10 between 2005-177T11:00 and 2005-177T16:00. Although the ring plane crossing was fully symmetric, the relative impact speed changed from 8.6 km s^{-1} before the crossing to 6.5 km s^{-1} after the crossing. This changed the mass of the particles reliably detected from 9.4×10^{-17} kg to 2.7×10^{-16} kg (from 0.28 μm radius to 0.4 μm radius assuming water ice particles). If the dust population is dominated by grains below 0.4 μm in radius, the rate profile can vary over orders of magnitude although the dust density might be constant.

For a conservative calculation of the dust density, the rates of the red and blue curves in the rate plots can be added and the sensitive area given in Table 4 and defined in Srama et al. (2004) can be used. The geometric information and the relative velocities are available on request or can be calculated from the Cassini spice kernels. For example a rate of 1 s^{-1}, a sensitive area of 0.05 m^2 and a common relative dust impact speed of 7 km s^{-1} refers to a dust density of 0.0028 m^{-3}. A maximum dust density of approximately 1 m^{-3} in the vicinity of Enceladus is therefore compatible with the rate measurements by DA.

A dust density profile along Cassini's trajectory was derived for the ring plane crossing on day 2005-122 in orbit 7 and is shown in Fig. 18. The dust density n (m^{-3}) is shown in dependence of radial distance from Saturn (x-axis, R_s) and height above the ring plane (y-axis, 10^3 km). The maximum density observed during this flyby was in the order of 0.5 m^{-3}. Please note that this is a rather conservative estimation and the real density might be much higher due to the limited impact rate measurement capabilities of the DA (dead time of 1 s). The curve in Fig. 18 takes into account Cassini's speed and the sensitive area of DA, but does not consider variations of the DA measurement thresholds caused by changes of relative dust impact speeds. A clear decrease of the dust density to further distances can be observed and density values below 0.0001 m^{-3} were observed at distances beyond 15R_s from Saturn. This figure is only one snapshop of the overall density in Saturn's environment and might not reflect the real nature and profile of Saturn's E-ring.

The dynamical information of the dust grains has to be derived from the dust flux profile modulated by DA boresight changes as they occurred during rolling and rocking downlinks. The result will be a set of dust orbital parameters at a given location within the ring. This analysis has been started and its results will be reported elsewhere.

6. Summary

In this paper we present the impact rate data provided by the DA instrument onboard Cassini. Measurements during the ring plane periapse orbit segments were investigated between Cassini's orbit insertion in July 2004 and July 2005. The DA impact rates showed a strong modulation with changes of the instrument boresight direction towards the dust RAM direction. The dust environment of Saturn is dominated by prograde particles on low-inclination orbits. Although the pointing variations lead to a fragmented data set, the dust environment was monitored between periapsis and distances up to 15R_s. Within approximately 7R_s and at low inclinations, the DA instrument measured rates above 1 s^{-1}. The dust density falls towards higher latitudes and greater distances. However, particles on bound and unbound orbits were found at altitudes as high as

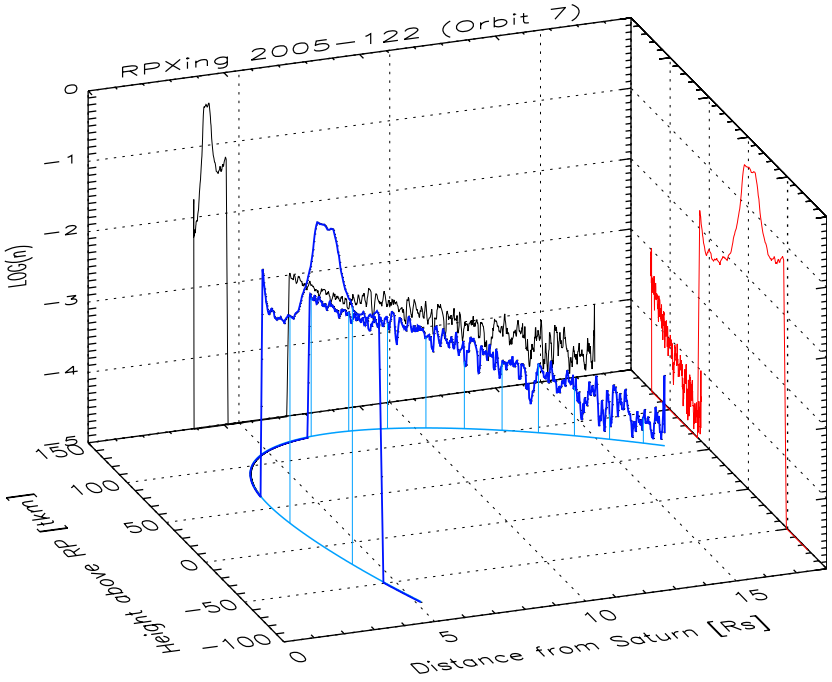

Fig. 18. Three-dimensional dust density profile (blue) along Cassini's trajectory of the ring plane crossing in orbit 7. Two projections of the density profile are shown on the side panels (black and red curve). The vertical axis gives the dust density n in units of m^{-3}.

120 000 km above the ring plane (17 latitude) and distances as far as $15R_S$. At elevations of 100 000 km above the ring plane dust densities of approximately $0.001\,m^{-3}$ were registered. The impact rates presented strongly indicate an extended E ring in both the vertical and horizontal directions. A superposition of the individual orbit segments and the calculation of the dust density profile is necessary in order to get the full picture of Saturn's dusty environment in three-dimensional space.

Finally, water ice particles were identified at high elevations above the ring plane and at large distances from Saturn.

Acknowledgements

This work has been supported by the Deutsches Zentrum für Luft- und Raumfahrt e.V. (DLR) under Grant 50 OH 0304.

References

Altobelli, N., Kempf, S., Landgraf, M., Srama, R., Dikarev, V., Krüger, H., Moragas-Klostermeyer, G., Grün, E., 2003. Cassini between Venus and Earth: detection of interstellar dust. J. Geophys. Res. 108, A10 LIS 7-1.

Bradley, J.G., Grün, E., Srama, R., 1996. The Cosmic Dust Analyzer for Cassini. Proceedings of SPIE, Denver, vol. 2803.

Gurnett, D.A., Grün, E., Gallagher, D., Kurth, W.S., Scarf, F.L., 1983. Micron-sized particles detected near Saturn by the Voyager plasma wave instrument. Icarus 53, 236–254.

Hillier, J.K., Green, S.F., McBride, N., Schwanethal, J.P., Srama, R., Kempf, S., Moragas-Klostermeyer, G., Postberg, F., McDonnell, J.A.M., Grün, E., 2006. The composition of Saturn's E ring, submitted for publication.

Howard, J.E., Dullin, H.R., Horanyi, M., 2000. Stability of halo orbits. Phys. Rev. Lett. 84 (15), 3244ff.

Kempf, S., Srama, R., Altobelli, N., Auer, S., Tschernjawski, V., Bradley, J., Burton, M.E., Helfert, S., Johnson, T.V., Krüger, H., Moragas-Klostermeyer, G., Grün, E., 2004. Cassini between Earth and asteroid belt: first in situ charge measurements of interplanetary grains. Icarus 171, 317–335.

Kempf, S., Srama, R., Postberg, F., Burton, M., Green, S.F., Helfert, S., Hillier, J.K., McBride, N., McDonnell, J.A.M., Moragas-Klostermeyer, G., Roy, M., Grün, E., 2005a. Composition of Saturnian Stream Particles. Science 307, 1274–1276.

Kempf, S., Srama, R., Horanyi, M., Burton, M., Helfert, S., Moragas-Klostermeyer, G., Roy, M., Grün, E., 2005b. High-velocity streams of dust originating from Saturn. Nature 433, 289–291.

Krüger, H., Krivov, A.V., Grün, E., 2000. A dust cloud of Ganymede maintained by hypervelocity impacts of interplanetary micrometeoroids. Planet. Space Sci. 48, 1457–1471.

Mitchell, C.J., Colwell, J.E., Horányi, M., 2005. Tenuous ring formation by the capture of interplanetary dust at Saturn. J. Geophys. Res. 110, A09218, doi:10.1029/2004JA010577.

Ockert-Bell, M.E., Burns, J.A., Daubar, I.J., Thomas, P.C., Veverka, J., 1999. The structure of Jupiter's ring system as revealed by the Galileo imaging experiment. Icarus 138, 188–213.

Postberg, F., Kempf, S., Srama, R., Green, S.F., Hillier, J.K., McBride, N., Grün, E., 2006. Composition of jovian stream particles. Icarus, revised.

Ratcliff, P.R., McDonnell, J.A.M., Firth, J.G., Grün, E., 1992. The Cosmic Dust Analyzer. J. Br. Interplanet. Soc. 45, 375–380.

Spahn, F., Thiessenhusen, K.-U., Colwel, J.E., Srama, R., 1999. Dynamics of dust ejected from enceladus: application to the Cassini dust detector. J. Geophys. Res. 104, 24111–24120.

Spahn, F., Schmidt, J., Albers, N., Hörning, M., Makuch, M., Seitz, M., Kempf, S., Srama, R., Dikarev, V., Helfert, S., Moragas-Klostermeyer, G., Krivov, A., Sremcevic, M., Tuzzolino, A., Economou, T., Grün, E., 2006. Cassini dust measurements at Enceladus: implications for Saturn's E ring. Science, revised.

Srama, R., Ahrens, T.J., Altobelli, N., Auer, S., Bradley, J.G., Burton, M., Dikarev, V.V., Economou, T., Fechtig, H., Görlich, M., Grande, M., Graps, A., Grün, E., Havnes, O., Helfert, S., Horányi, M., Igenbergs, E., Jessberger, E.K., Johnson, T.V., Kempf, S., Krivov, A.V., Krüger, H., Mocker-Ahlreep, A., Moragas-Klostermeyer, G., Lamy, P., Landgraf, M., Linkert, D., Linkert, G., Lura, F., McDonnell, J.A.M., Möhlmann, D., Morfill, G.E., Müller, M., Roy, M., Schäfer, G., Schlotzhauer, G., Schwehm, G.H., Spahn, F., Stübig, M., Svestka, J., Tschernjawski, V., Tuzzolino, A.J., Wäsch, R., Zook, H.A., 2004. The Cassini Cosmic Dust Analyzer. Space Sci. Rev. 114, 465–518.

Further reading

Dikarev, V.V., 1999. Dynamics of particles in Saturn's E ring: effects of charge variations and the plasma drag force. Astron. Astrophys. 346, 1011–1019.

Hamilton, D.P., 1993. Motion of dust in a planetary magnetosphere: orbit-averaged equations for oblateness, electromagnetic, and radiation forces with application to Saturn's E ring. Icarus 101, 244–264.

Horányi, M., Burns, J.A., Hamilton, D.P., 1992. The dynamics of Saturn's E-ring particles. Icarus 97, 248–259.

Kempf, S., Beckmann, U., Srama., R., Horányi, M., Auer, S., Grün, E., 2006. The electro-static potential of E ring particles. Planet. Space Sci., submitted for publication.

Srama, R., Grün, E., 1997. The dust sensor for Cassini. Adv. Space Res. 20 (8), 1467–1470.

Showalter, M.R., Cuzzi, J.N., Larson, S.M., 1991. Structure and particle properties of Saturn's E Ring. Icarus 94, 451–473.